

This document was prepared in conjunction with work accomplished under Contract No. DE-AC09-96SR18500 with the U. S. Department of Energy.

DISCLAIMER

This report was prepared as an account of work sponsored by an agency of the United States Government. Neither the United States Government nor any agency thereof, nor any of their employees, nor any of their contractors, subcontractors or their employees, makes any warranty, express or implied, or assumes any legal liability or responsibility for the accuracy, completeness, or any third party's use or the results of such use of any information, apparatus, product, or process disclosed, or represents that its use would not infringe privately owned rights. Reference herein to any specific commercial product, process, or service by trade name, trademark, manufacturer, or otherwise, does not necessarily constitute or imply its endorsement, recommendation, or favoring by the United States Government or any agency thereof or its contractors or subcontractors. The views and opinions of authors expressed herein do not necessarily state or reflect those of the United States Government or any agency thereof.

WSRC-TR-99-240, Rev. 0

**Keywords: waste glass,
crystallization, statistical process
control**

QUASICRYSTALLINE APPROACH TO PREDICTING THE SPINEL-NEPHELINE LIQUIDUS: APPLICATION TO NUCLEAR WASTE GLASS PROCESSING

Carol M. Jantzen
Savannah River National Laboratory
Aiken, SC 29808

and

Kevin G. Brown[†]
Savannah River National Laboratory
Aiken, SC 29808

For publication only in the Journal of the American Ceramic Society

Savannah River National Laboratory
Aiken, SC 29808



Prepared for the U.S. Department of Energy Under Contract Number
DEAC09-96SR18500

[†] current address Department of Civil and Environmental Engineering, Vanderbilt University,
Nashville, TN 37235

QUASICRYSTALLINE APPROACH TO PREDICTING THE SPINEL-NEPHELINE LIQUIDUS: APPLICATION TO NUCLEAR WASTE GLASS PROCESSING

Carol M. Jantzen
Savannah River National Laboratory
Aiken, SC 29808
(carol.jantzen@srnl.doe.gov)

Kevin G. Brown[†]
Savannah River National Laboratory
Aiken, SC 29808
kevin.g.brown@vanderbilt.edu

ABSTRACT

The crystal-melt equilibria in complex fifteen component melts are modeled based on quasicrystalline concepts. A pseudobinary phase diagram between acmite (which melts incongruently to a transition metal ferrite spinel) and nepheline is defined. The pseudobinary lies within the $\text{Al}_2\text{O}_3\text{-Fe}_2\text{O}_3\text{-Na}_2\text{O-SiO}_2$ quaternary system that defines the crystallization of basalt glass melts. The pseudobinary provides the partitioning of species between the melt and the primary liquidus phases. The medium range order of the melt and the melt-crystal exchange equilibria are defined based on a constrained mathematical treatment that considers the crystallochemical coordination of the elemental species in acmite and nepheline. The liquidus phases that form are shown to be governed by the melt polymerization and the octahedral site preference energies. This quasicrystalline liquidus model has been used to prevent unwanted crystallization in the world's largest high level waste (HLW) melter for the past three years while allowing >10 wt% higher waste loadings to be processed.

I. INTRODUCTION

Processing of High-level radioactive wastes (HLW) into borosilicate glass began in the United States in 1996 in Aiken, SC (the Defense Waste Processing Facility, DWPF) and in West Valley, NY (the West Valley Demonstration Project, WVDP) [1,2,3]. A third Joule heated waste glass melter is currently being constructed in Richland, WA [2] at the Hanford Waste Treatment Plant (WTP). Vitrification of HLW wastes in the UK [4] and France [5,6] have been ongoing for ~ 20 years and vitrification facilities are planned in Germany [7].

The DWPF is currently the largest HLW waste glass vitrification facility in the world. Since 1994, the DWPF vitrification process has been controlled using a statistical process control system known as the Product Composition Control System (PCCS) [8,9]. The PCCS utilizes individual product and process control models [10,11,12,13], to simultaneously ensure that the waste glass is durable, homogeneous (not phase separated), and pourable, as well as eliminating the potential for crystallization of the primary liquidus phase(s) in the melt pool during routine operation.

[†] current address Department of Civil and Environmental Engineering, Vanderbilt University, Nashville, TN 37235

Crystallization in the melt pool during routine operation would be problematic since large insoluble crystals can settle to the floor of the melter and partially or completely block the pour spout.^f The presence of crystals also causes the melt to be non-Newtonian and causes the viscosity of the melt to increase [14,15]. Increased viscosity may cause difficulty in discharging the glass from the melter. The presence of crystals in the melt can also cause the resistivity of the glass to rise, which can make melting of the glass more difficult [15]. If crystallization accumulates on the melter floor at the height of the electrodes, the melt pool will no longer be able to sustain Joule heating and the melt pool can solidify [14,16,17,18,19].

There are two principal types of crystallization that can occur in a waste glass melter:

- *Surface crystallization* where crystal growth nucleates at the melt-atmosphere or the melt-refractory interface and grows perpendicular to this interface [20]
- *Volume crystallization* where crystal growth begins from homogeneous or heterogeneous nucleation sites within a melt [20]
 - volume crystallization of spinel in waste glasses has been shown to be heterogeneous, forming on melt insolubles such as RuO₂, Ag^o, Pt^o present in the waste [21, 22]

Surface crystallization is not problematic in nuclear waste glass melters since spinel precursors (NaFe₂O₄ and LiFe₂O₄), which can redissolve in the melt pool, have been found to form at the melt-atmosphere interface [14,23]. Moreover, waste glass melts have been found to form a spinel rich protective layer along the chrome rich refractory walls which then minimizes spinel formation in the melt pool from the refractory surfaces [24] as long as the protective layer is not removed by melt pool agitation or bubbling.

Volume crystallization, on the other hand, can involve rapid nucleation of the melt pool. Once formed, the NiFe₂O₄ spinel crystals that form are refractory and cannot be redissolved into the melt pool at the operating temperature of 1150°C. Therefore, liquidus temperature modeling has focused on heterogeneous volume crystallization rather than on surface crystallization.

The fundamental approach to the development of the product quality and process models needed to control the critical properties (e.g. durability, liquidus temperature, melt viscosity, etc.) for processing compositionally diverse nuclear wastes has been to relate these properties to rational functions of glass composition. The rational functions of glass composition used in PCCS represent mechanistic or structural properties of the glass. For liquidus, the current PCCS model represents the glass-crystal equilibrium. Mechanistic models are preferred over empirically derived models [25] and allow greater flexibility in application to process control.

Higher waste loadings (generally rich in Fe₂O₃ and alkali) can promote crystallization but higher waste loadings are desirable because they allow more waste to be processed per canister, producing fewer canisters for ultimate storage in a geologic repository and lowering disposal and operating costs. Because of the cost incentives associated with simultaneously maximizing waste loading while preventing unwanted crystallization in high level waste melters, there have

^f bubbling or stirring a melt pool may make small crystals buoyant enough not to accumulate in the melter and be flushed out with the glass that is poured but growth of larger crystals during process outages when the melt pool is idled may still be problematic.

been many liquidus models developed. Due to the complexity of the ~15 oxide component nuclear waste glasses, liquidus models here-to-fore developed have been primarily empirical [26,27,28,29] or extremely simple mechanistic models based on only a few melt components [10,30].

The focus of this study is to develop a comprehensive mechanistic/structural model that expresses crystallization of the two most commonly observed primary liquidus phase(s), e.g. spinel and nepheline, in terms of a consistent pseudobinary phase diagram. Since the borosilicate waste glasses are similar in composition to basalt glass on a borate free basis and since no borate phases crystallize on the liquidus, the crystallization chemistry of the waste glasses can be described by the known phase relations of the geochemical basalt quaternary $\text{Fe}_2\text{O}_3\text{-Al}_2\text{O}_3\text{-SiO}_2\text{-Na}_2\text{O}$ system [31] or the reduced iron $\text{Fe}_3\text{O}_4\text{-Al}_2\text{O}_3\text{-SiO}_2\text{-Na}_2\text{O}$ system [32]. The first PCCS liquidus model developed [10] was based on the equilibria in the $\text{Fe}_2\text{O}_3\text{-Al}_2\text{O}_3\text{-SiO}_2\text{-Na}_2\text{O}$ system [31] and this system was also used to develop a basic understanding of phase separation in waste glasses [33] and the impacts of quasichemical glass structures on waste glass durability [34].

The present study will attempt to link the macroscopic phase assemblages crystallizing at the liquidus to their medium range order (MRO) state in the melt to address the following: (1) how do the network modifying cations apportion between anionic structural groups such as $(\text{SiO}_4)^{-4}$, $(\text{AlO}_4)^{-5}$, $(\text{FeO}_4)^{-5}$, $(\text{BO}_4)^{-5}$ and $(\text{BO}_3)^{-3}$, (2) what is the role of the melt polymerization in terms of Q distributions, and (3) what is the role of the octahedral site preference energies in crystalline phase formation. Because the pertinent thermodynamic data does not exist for these complex systems, a coupled quasicrystalline and mathematical approach is used to apportion cations with anionic groups and to model the liquidus (crystal-liquid) equilibrium based on these quasicrystalline species.

II. PREVIOUS WORK

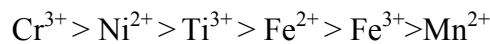
(1) Identification and Analyses of Primary Liquidus Phases

The primary liquidus phase(s) in nuclear waste glasses have either been determined during conventional liquidus measurement [35,36] or during the development of time-temperature-transformation (TTT) curves [21, 22, 37,38]. Table I summarizes the liquidus primary phases commonly observed. The table summarizes the pertinent species present and spans high Al_2O_3 containing glasses to high Fe_2O_3 containing glasses and high alkali (Li_2O and/or Na_2O) to high ZrO_2 and ThO_2 containing glasses. For waste glass components such as ZrO_2 , ZrSiO_4 , ThO_2 , CeO_2 that are stoichiometric and exhibit little solid solution, solubility limits can be placed on the glass composition so that these liquidus primary phases do not form. For liquidus primary phases such as spinel and nepheline that vary widely in composition and elemental substitution of transition metals, alkali oxides, and alkaline earth oxides, compositionally dependent liquidus models are needed.

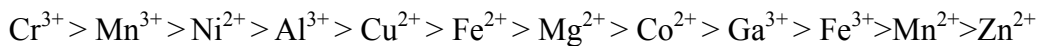
Spinel is the primary liquidus phase in >65% of the waste glasses studied followed by nepheline. Clinopyroxenes of the acmite($\text{NaFe}_2\text{Si}_2\text{O}_6$)-augite ($\text{Ca,Na,Mg,Fe}^{2+},\text{Mn,Fe}^{3+},\text{Al,Ti}_2[(\text{Si,Al})_2\text{O}_6]$) and hedenbergite($\text{CaFe}^{2+}[\text{Si}_2\text{O}_6]$)-diopside($\text{CaMg}[\text{Si}_2\text{O}_6]$) type sometimes appear as liquidus

phases (Table I) as do the orthopyroxenes enstatite-ferrosilite solid solutions, $(\text{Mg,Fe}^{+2})\text{SiO}_3$. Occasionally, olivine $(\text{Mg,Fe})_2\text{SiO}_4$, ZrSiO_4 , $\text{Na}_4\text{Zr}_2\text{Si}_3\text{O}_{12}$, or $\text{Ca}_2\text{ZrSi}_4\text{O}_{12}$ have formed in Mg or Zr rich waste glass melts that are unusually low in SiO_2 and/or in the absence of sufficient iron (≤ 4.5 wt%) [28], a major component of most high level waste (HLW) glass melts that encourages the formation of the acmite-augites which incongruently melt to ferrite rich spinels. The olivines and orthopyroxenes are only favored when the melt is enriched in MgO [28].

The spinel liquidus phase that crystallizes from HLW waste glass melts is nominally NiFe_2O_4 , an inverse BABO_4 spinel structure [39], where all the divalent elements ($^{[6]}\text{B}=\text{Mg}^{2+}$, Zn^{2+} , Fe^{2+} , Ni^{2+})^{††} are in octahedral coordination and half of the Fe^{3+} are in octahedral coordination ($^{[6]}\text{B}$) while the remaining Fe^{3+} are tetrahedrally coordinated in the $^{[4]}\text{A}$ lattice site. Small amounts of Cr^{3+} and Al^{3+} substitution, and occasionally substitution of Ti^{4+} or Ti^{3+} [40], can occur in these inverse spinels. However, the remaining aluminate and chromite spinels and MnFe_2O_4 spinels have a normal spinel structure in which all of the +3 species prefer the octahedral sites and the Mn^{2+} occupies the $^{[4]}\text{A}$ lattice site. This is because the excess octahedral site preference energy (OPSE), which is a measure of the preference of any ion for the octahedral site, diminishes in the following order for spinels [39]:



The ordering of diminishing OSPE in kcal was experimentally determined for a wide variety of spinels by Navrotsky and Kleppa [41] and shown to be:



Conversley, the elements from Mg^{2+} to Zn^{2+} show an increasing tendency for tetrahedral site preference in the order $\text{Zn}^{2+} > \text{Mn}^{2+} > \text{Fe}^{3+} > \text{Ga}^{3+} > \text{Co}^{2+} > \text{Mg}^{2+}$.

The spinels observed in high iron containing waste glasses [42] were analyzed by microprobe and found to be 85-95% NiFe_2O_4 (see oxidized and reduced 165TDS-U glasses in Table II). Subsequent studies [28] (Glass SS-A in Table II) confirmed that the spinel composition was predominately NiFe_2O_4 spinel containing only 3% Mn and 0.9% Mg, ~25% Cr^{3+} , 2% Al, and 2% Si. For borosilicate waste glass compositions relevant to the disposal of Hanford wastes [43] the primary phase was also a NiFe_2O_4 type spinel but the Ni was determined to vary between 53-74%, Mn between 5-7%, Fe^{2+} between 0.21-0.42%, Fe^{3+} between 31-91%, and Cr between 9-69% depending on the SiO_2 content of the glass matrix (Table II).

Nepheline can also appear as a primary liquidus phase in waste glasses that are simultaneously high in Al_2O_3 and Na_2O [22,44,45]. Nepheline is an SiO_2 framework structure in which approximately half of the silicon atoms are replaced by aluminum forming voids which are normally filled with Na [46]. The voids can also be vacant (\square), partially filled by K or Ca and the general formula is expressed as $^{[9]}\text{K}_x^{[8]}\text{Na}_y^{[8]}\text{Ca}_z^{[8]}\square_{8-(x+y+z)}^{[4]}\text{Al}_{(x+y+2z)}^{[4]}\text{Si}_{16-(x+y+2z)}\text{O}_{32}$ [47]. Electron microprobe analyses of nepheline formed as a primary liquidus phase from a simulated HWVP waste glass is given in Table II and shown to have considerable vacancies and

†† Notation such as $^{[6]}\text{B}$ and $^{[4]}\text{A}$ will be used to designate the coordination of the lattice sites, in this case octahedral ([6]) coordination for the B lattice site and tetrahedral ([4]) coordination for the A lattice site.

considerable substitution of Fe^{3+} for Al and Si in the framework structure. There is evidence that the primary liquidus phase spinel may persist metastably and/or nucleate nepheline crystallization, since the two phases are often found together as primary liquidus phases and microscopy has shown that primary phase nepheline has inclusions of spinel [44]. The presence of TiO_2 in a glass is also known to preferentially cause nucleation of nepheline in glass [48] and Ti in nepheline is primarily tetrahedral [46].

The clinopyroxenes (disilicates) minerals have the general formula $\text{M}_2\text{M}_1[\text{T}_2\text{O}_6]$ where the distorted 6 to 8 coordinated $^{[6-8]}\text{M}_2$ sites can be occupied by Ni, Mg, Mn, Ca, K, Li, or Na, while the regular 6 coordinated $^{[6]}\text{M}_1$ sites can be occupied by Mn, Mg, Ni, Zr, Cr, Ti, Fe or Al and the tetrahedral $^{[4]}\text{T}$ sites by Si, Al or Fe^{3+} [49]. The $^{[6-8]}\text{M}_2$ sites can accommodate larger cations, such as Na and Ca versus the $^{[6]}\text{M}_1$ sites. Acmite, nominally $\text{NaFeSi}_2\text{O}_6$, is frequently found in DWPF glasses but it is not a primary liquidus phase. The acmite typically takes on one of two melt structures, appearing to grow from nickel iron spinel or from RuO_2 insoluble phases during cooling [42]. An analysis of the Ni rich acmite typically found in DWPF type waste glasses of ~1 wt% NiO is given in Table II. The analysis of a primary phase clinopyroxene from a DWPF type waste glass containing <0.06 wt% NiO and enriched in CaO and MgO over the nominal amounts in these glasses (Glass SG02 in Table II), indicated that compositionally it was ~50% augite and ~50% acmite. ‡ For Hanford type borosilicate glasses, which cover a wider composition range than the DWPF glasses, the clinopyroxene primary phases hedenbergite ($\text{CaFe}^{2+}[\text{Si}_2\text{O}_6]$) and diopside ($\text{CaMg}[\text{Si}_2\text{O}_6]$) have been associated with the absence of transition metal species such as Ni^{2+} and higher concentrations of Mg^{2+} and Ca^{2+} [28, 29]. Excess B_2O_3 in waste glasses (>12 wt%) was found to suppress the formation of clinopyroxene crystals [28], ratios of $(\text{Na}+\text{K})/\text{Al} > 1$ were found to stabilize acmite over augite, and the presence of TiO_2 was found to stabilize augite over acmite [50].

No radioactive species have been observed as primary liquidus phases in the 366 glasses studied (Table I). Spinel appears as the primary liquidus phase in WVNS glasses even though these glasses contain approximately 3.6 wt% ThO_2 . Solid solutions of ThO_2 - CeO_2 crystallize ~150°C below the liquidus temperature [51]. There is microscopy and electron microprobe evidence that the ThO_2 and ThO_2 - CeO_2 solid solutions nucleate on the spinel primary phase [51,52]. CeO_2 was found to precipitate from certain waste glasses when present in excess of 3 wt% [53]. There is no experimental evidence that UO_2 or any other uranium containing phase forms as a primary liquidus phase † in glasses containing up to 4.2 wt% UO_2 [22].

(2) Phase Equilibria and Quasichemical Liquidus Modeling

A mechanistic model for spinel crystallization has been proposed by Vienna, et. al.[54] which includes 15 individual components and 7 empirically fit parameters. This mechanistic model is based on the ionic potential of the glass components (estimated by their short range order, SRO, assuming that the SRO ionic radii are the same as published values for crystalline ionic radii).

‡ a solid solution series exists between the Na (acmite) and Ca (augite) rich end members of this clinopyroxene series.

† UO_2 has been observed as a crystallization product that forms at annealing times of >40 hours at temperatures $\leq 700^\circ\text{C}$.

The model appears highly accurate for liquidus data from waste glass compositions from which it was derived, e.g. Hanford waste glasses, but it does not adequately predict spinel liquidus temperatures for the extreme matrix data presented in this study nor for many of the glasses used for model validation.

Liquidus and/or crystallization models that are based on binary, ternary, or quaternary phase equilibria, include the first PCCS model for spinel [10], the Plodinec model for $\text{Ni}(\text{Cr,Fe})_2\text{O}_4$ spinel [30] as well as the Li [55] and the Bessman [56] models for nepheline. In addition, Pelton [57] and Pelton and Blander [58,59] have developed quasichemical equations to express the thermodynamic properties of ordered liquid solutions such as silicate slags and applied these to the computer generation of binary and ternary oxide liquidus surfaces and to 15 component waste glasses. The quasichemical equations take into account the concentration and temperature dependence of the melt properties, of ordered systems.

The first PCCS three component model assumed a binary equilibrium existed between spinel and nepheline in the $\text{Fe}_2\text{O}_3\text{-Al}_2\text{O}_3\text{-SiO}_2\text{-Na}_2\text{O}$ system. The first PCCS model was influenced by previous studies [60] which developed a pseudobinary phase diagram for the system magnetite spinel $((\text{Fe}^{+2}\text{Fe}_2^{+3}\text{O}_4)\text{-UO}_2)$ used to clean core debris at Three Mile Island (TMI). The Plodinec solubility model [30] assumed that simple binary solutions existed in the $\text{NiO-Fe}_2\text{O}_3$ or $\text{NiO-Cr}_2\text{O}_3$ system depending on whether iron rich or chromium rich spinel formed as the primary phase. This model did not allow for mixed $\text{NiO-Fe}_2\text{O}_3\text{-Cr}_2\text{O}_3$ spinel formation.

Li [55] developed a method for the prediction of nepheline as the primary crystalline phase during canister cooling for Hanford waste glass compositions. Simply stated, if the glass composition, normalized to the $\text{Na}_2\text{O-Al}_2\text{O}_3\text{-SiO}_2$ (NAS) system, fell within the nepheline phase field in the known ternary phase diagram then the glass would crystallize nepheline. Li's model did not perform well when modeled against liquidus temperature and hence an empirically derived model was subsequently developed [44]. More recently, Bessmann, et. al. [56] used a thermochemical approach to model the nepheline binary liquidus between nepheline- SiO_2 in the NAS ternary system and found good agreement between the model and the experimentally determined nepheline- SiO_2 join. The thermochemical model was then extended to modeling Li's data in the NAS system and to calculate the effects of additional SiO_2 and B_2O_3 on the formation of nepheline in waste glasses. The thermochemical approach does not take into account the effects of Fe^{3+} that is known [45] to substitute in the nepheline lattice, nor the effects of Ti and other alkali on the crystallization of the nepheline phase. Likewise, simple $\text{NiO-Fe}_2\text{O}_3$ spinels can be modeled using the thermochemical approach as binary systems but not complex Ni-Fe-Cr-Mn-Mg containing spinels.

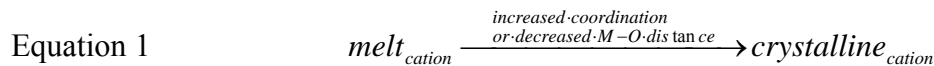
The Pelton [57] quasichemical approach generated a regression to 15 component waste glasses. Many species that are not observed to form as a primary liquidus phases in waste glasses are predicted to form, e.g. anorthite, albite, lithium aluminum silicate, corundum (a solid solution of $\text{Al}_2\text{O}_3\text{-Fe}_2\text{O}_3\text{-Cr}_2\text{O}_3$) and olivine to name a few. Conversely, the ubiquitous spinel (of the Ni-Fe-Cr-Mn-Mg type) and nepheline primary phases are not predicted phases to form. This is because the thermodynamic quasichemical approach assumes phase pure oxide end members and intermediates (quasichemical clusters such as MgSiO_3). This is a necessity of the methodology

which minimizes the Gibbs free energy and necessitates that the Gibbs free energy as a function of temperature be known for the end members used in modeling.

(3) Role of Medium Range Order (MRO) or Quasicrystals in Glass

Borosilicate waste glasses and melts, like natural silicate glasses and melts, possess short-range order (SRO; radius of influence $\sim 1.6\text{-}3\text{\AA}$) around a central atom, e.g. polyhedra such as tetrahedral and octahedral structural units [61]. Glasses also possess MRO [61] which encompasses second- and third-neighbor environments around a central atom (radius of influence $\sim 3\text{-}6\text{\AA}$). The more highly ordered regions, referred to as clusters or quasicrystals, often have atomic arrangements that approach those of crystals [61,62].

When the MRO in a glass or melt becomes enough like that of a crystalline phase, nucleation and crystal growth may occur given a sufficient energy drive such as undercooling [61].[‡] Williams [63] was the first (1959) to suggest that the partitioning of a cation from melt to crystal, e.g. at the liquidus, usually involves an increase in the average coordination number and a decrease in the average atomic distance of a cation as given in



In particular, transition metal ions, which have large polarization energies, will gain energy on transfer from the liquid to the solid phase due to the shortening of the interatomic distances, e.g. by leaving sites of irregular coordination in the melt for regular octahedrally coordinated sites in a crystalline structure. This has been confirmed by recent experiments that cations occupy fewer octahedral sites in the melt than in the coexisting crystal [64]. This OSPE tendency can be calculated and/or measured for simple systems [65]. For example, measurements of glass and melt structures have demonstrated that the coordination of Ni is octahedral ($^{[6]}\text{Ni}$) in crystalline silicates, pentahedral ($^{[5]}\text{Ni}$) in silicate glasses, and tetrahedral ($^{[4]}\text{Ni}$) in silicate melts, e.g. the assumption that the structure of a glass is the same as that of its melt or the crystalline species from which it was derived is not always true [61]. Specifically, the simple concept of using bond lengths and bond strength from SRO parameters for crystalline species is not always appropriate to the domain for MRO or quasicrystals in glass because the bond lengths expand and the coordination of the cation changes as a function of temperature. This may be a short coming of the recently developed SRO ion potential model for modeling liquidus temperature in waste glasses [54].

The existence of MRO in melts and glasses led to a redefinition [66] of the widely accepted Zachariasen-Warren random-network structure model of glass [67,68,69] and its predecessor the crystallite structure model of glass [70]. The “modified crystallite model” of glass structure treats the degree of medium-range order as spatial fluctuations in the glass network [66]. Similarly, Greaves [71] proposed a “modified random network (MRN)” model which involves two interlacing “sublattices.” One sublattice is more highly ordered (network regions) while the

[‡] see Section V.6

other is not (inter-network regions made up of large concentrations of network modifiers). The MRN model is able to describe the existence of large cation rich clusters in glass, e.g. clusters of Ca in CaSiO_3 glasses [71].

MRO in glasses and melts has been measured for many single component mineral melts and glasses, e.g. SiO_2 glass [61] and nepheline glass [72], as well as in complex natural silicate melts [61]. For example, the formation of nuclei (clusters or quasicrystals) of Ni-diopside, $(\text{Ca,Mg,Ni})_2\text{Si}_4\text{O}_{12}$, were observed in situ near 1100K in a diopside composition glass containing 2 wt% Ni [73]. Thus both structurally and thermodynamically, the liquidus represents a boundary between phases of contrasting degrees of polymerization in a melt [74].

Examples of MRO are repetitive arrangements of corner-linked polyhedra, such as silicate tetrahedra with four bridging oxygens attached to neighboring silica tetrahedra (Q^4 units), or six or eight membered rings or sheets of corner-linked silicate tetrahedra. Here, the polymerization notation from ^{29}Si NMR spectroscopy is used to designate the number of bridging oxygens for a given silica tetrahedra as a superscript. The polymerization or extent of MRO of a melt can thus be expressed by calculating [75] or measuring [76] a Q distribution, e.g. the number of Q^4 , Q^3 , Q^2 , Q^1 , and Q^0 species in the melt. For example, Smart and Glasser [76] measured Q^1 (SiO_4), Q^2 (Si_2O_7), Q^3 (Si_3O_9 cyclic trimers and Si_3O_{10} chains), Q^4 (Si_4O_{12} four membered rings and Si_6O_{18} six membered rings or clusters) species in PbO-SiO_2 glasses containing between 55-90 mol% PbO .

The number of Q^4 units in a melt, e.g. silica tetrahedra that have not reacted with a metal cation to form a non-bridging oxygen, can be correlated to the thermodynamic activity of SiO_2 in the melt [77]. The Q distribution in a glass has been shown to also influence freezing point depression of a glass, i.e. the liquidus, as well as crystallization rate and phase separation [77]. In particular, a bimodal Q distribution will promote phase separation while systems which have larger concentrations of Q^0 and Q^1 species (more modifier rich) will crystallize more rapidly than melts with oxides which produce primarily Q^3 . Systems with lower temperature liquidus curves have been shown to have lower concentrations of low Q species and hence crystallize more slowly [77].

Recent studies have shown that the solution properties of cations in multicomponent silicate melts not only depend upon Q distribution or the Si:O ratio, but also on the identities and concentrations of the other cations in the melt, particularly the highly charged cations of high field strengths [78]. One approach has been to model the microstate of a melt as a homogeneous equilibrium between polyhedral complexes formed between silicate anionic groups and their network-modifying cations [78]. Thermodynamic data from glasses and melts have been used to establish a hierarchy of the relative stability of aluminum-bearing silicate clusters or quasicrystals in melts. The stability of the aluminate groups are $\text{KAlO}_2 > \text{NaAlO}_2 > \text{LiAlO}_2 > \text{Ca}_{0.5}\text{AlO}_2 > \text{Fe}_{0.5}\text{AlO}_2 > \text{Mg}_{0.5}\text{AlO}_2$ [74]. Qualitatively, the behavior of tetrahedrally coordinated Fe^{3+} resembles that of Al^{3+} in that it requires electrical charge-balance with alkali metals, alkaline earths or ferrous iron [74]. The hierarchy for Fe^{3+} complexes suggested by Mysen [74] is similar to that of the aluminate complexes, e.g. $\text{KFeO}_2 > \text{NaFeO}_2 > \text{LiFeO}_2 > \text{Ca}_{0.5}\text{FeO}_2 > \text{Fe}_{0.5}\text{AlO}_2 > \text{Mg}_{0.5}\text{FeO}_2$. Since both Al^{3+} and Fe^{3+} in tetrahedral coordination need to be charge

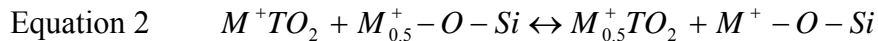
balanced, and the relative stability of the Al^{3+} and Fe^{3+} complexes is considered to be the same, the convention is to first assign cations to the ferric iron complexes [74].

(4) Identification of Quasicrystals in Nuclear Waste Glasses

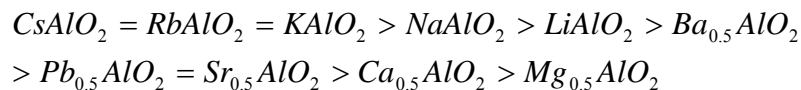
In 1990, Ellison and Navrotsky [79] studied a DWPF average composition glass representative of the first radioactive waste glass to be processed in the DWPF (Blend 1). Based on studies in natural analog systems, the authors concluded that this waste glass should be composed of the following polymerized tetrahedral groups: ~5.2 mole% $(\text{K,Na,Li})\text{AlO}_2$, ~5.8 mole% $(\text{K,Na,Li})\text{FeO}_2$, ~15.3 mole% $(\text{K,Na,Li})\text{BO}_2$, and ~55.4 mole% SiO_2 . The approximately 10 mole% minor components such as NiO , FeO , MnO , MgO , CaO , TiO_2 and excess $(\text{K,Na,Li})_2\text{O}$ over that needed to stabilize the B^{3+} , Al^{3+} , and Fe^{3+} tetrahedral units were ignored. The excess $(\text{K,Na,Li})_2\text{O}$ in this waste glass suggests that network-modifier-rich polymerization dominates over silica-rich polymerization [79]. This is an important distinction relative to possible quasicrystalline reactions governing liquidus crystallization.

Ellison and Navrotsky [79] hypothesized that the hierarchy for polymerization for Na^+ tetrahedral groups in DWPF type glasses would be $\text{NaBO}_2 > \text{NaFeO}_2 > \text{NaAlO}_2$. The following was also noted regarding DWPF type glasses:

- some fraction of the tetrahedral $[\text{T}^{3+}]$ cations (Al^{3+} , Fe^{3+} , B^{3+}) must be charge-balanced by divalent cations, setting up an equilibrium represented by Equation 2



- divalent cations were predicted to compete more effectively with Al^{3+} for available oxygen than monovalent cations: this reduces the stability of potential $M_{0.5}^+ \text{TO}_2$ complexes
- the hierarchy governing the formation of $M^+ \text{AlO}_2$ and $M_{0.5}^{2+} \text{TO}_2$ complexes suggested was



- highly charged +4, +5, and +6 cations in the excess modifier waste glasses was hypothesized to allow oxide species such as TiO_2 , ZrO_2 , and SnO_2 to form local alkali-titanate, alkali-zirconate, or alkali-stannate polymerized groups with nearly stoichiometric compositions, e.g. Na_2TiO_3 or CaTiO_3 .

Experimental evidence for the existence of alkali ferric iron clusters (NaFeO_2 and LiFeO_2 complexes) in nuclear waste glasses is supported by the x-ray identification of NaFe_2O_4 and LiFe_2O_4 spinel structured crystallites during the melter feed to glass conversion. The alkali ferric iron clusters have been observed in both pilot scale melter tests [14] and crucible tests [23].

These alkali ferric iron clusters appear to contain no Ni or Cr and are transient in the melt later converting to $\text{Ni(Fe,Cr)}_2\text{O}_4$ spinels [14,23,80].

Experimental evidence for $(\text{Na,K,Li})\text{BO}_2$ structural groups in the melt is supported by mass spectrometric analyses of $(\text{Na,Li})\text{BO}_2$ vapors [81,82] present above simulated waste glass melts at temperatures between 800-1150°C, e.g. $(\text{Na,Li})\text{BO}_2$ in the melt must be in equilibrium with $(\text{Na,Li})\text{BO}_2$ in the vapor [83].

The existence of NaAlO_2 clusters or quasicrystals has been studied in simulated nuclear waste glasses by Li [84,45]. This Raman spectroscopy study of nuclear waste glasses prone to form nepheline as the primary liquidus phase demonstrated that these quenched glasses contained discrete clusters of $[\text{NaAlSiO}_4]$ units. Indeed, the 850 cm^{-1} vibration in the spectra, characteristic of the $[\text{NaAlSiO}_4]$ clusters was shown to correlate to the measured liquidus temperature of these glasses yielding a correlation with an R^2 value of 0.98. Li's findings were similar to the results [72] obtained by X-ray radial distribution function (RDF) analysis on pure nepheline glass and the results of molecular dynamics simulations of glasses in the $\text{NaAlSiO}_4\text{-SiO}_2$ system [85]. Pure nepheline glass was shown to have a stuffed tridymite-like structure (six-membered rings of silica tetrahedra) similar to that of crystalline nepheline. Li's conclusions about nepheline rich nuclear waste glasses are:

- increasing the concentration of Na_2O in a high Al_2O_3 containing waste glasses increases the concentration of NaAlO_2 nepheline forming groups
- increasing the SiO_2 content decreases the tendency of $[\text{NaAlSiO}_4]$ formation by diluting the number of available NaAlO_2 nepheline forming groups
- increasing the B_2O_3 content of the glass allows the Na_2O to preferentially bond to the B_2O_3 forming NaBO_2 groups decreasing the number of available NaAlO_2 nepheline forming groups
- the effect of increasing B_2O_3 was stronger than increasing SiO_2 on inhibiting the formation of nepheline forming groups

Experimental evidence for transition metal-silicate structures is supported by the Raman spectroscopy and optical absorption spectroscopy of Nelson, Furukawa and White [86].

III. EXPERIMENTAL

(1) Quasicrystalline Glass Experiments

In order to evaluate the preferred partitioning between the divalent and trivalent transition metals (Cr^{3+} , Ni^{2+} , Fe^{2+} , Fe^{3+} , Mn^{2+} , and Al^{3+}) and the OSPE between the melt and the spinel liquidus phases, glasses containing individual divalent-trivalent pairs were examined, e.g. $\text{Ni}^{2+}\text{-Cr}^{3+}$ was examined in the absence of $\text{Ni}^{2+}\text{-Fe}^{3+}$ and vice versa (Table III). In order to examine the role of Al^{3+} , the $\text{Ni}^{2+}\text{-Cr}^{3+}$ and $\text{Ni}^{2+}\text{-Fe}^{3+}$ pairs were examined in the absence and presence of Al^{3+} . In

addition, the formation of phases in the absence of Cr^{3+} and Fe^{3+} were examined, e.g. Ni^{2+} - Al^{3+} , Fe^{2+} - Al^{3+} , Mg^{2+} - Al^{3+} , and Mn^{2+} - Al^{3+} pairs.

Glasses were made from an average DWPF (Stage I) waste and a borosilicate frit (F202). Glasses were melted for 4 hours in Pt crucibles at the melt temperature of 1150°C and at the DWPF liquidus control temperature of 1050°C . The Fe_2O_3 in the Fe^{3+} only experiments varied from 18.02 to 19.97 wt% while the Fe_2O_3 in the Fe^{3+} - Al^{3+} coupled experiments varied from 19.49 to 21.55 wt% with an Al_2O_3 content of 7.1-7.5 wt%. The Cr_2O_3 in the Cr^{3+} only experiments varied from 19.3 to 19.97 wt% while the Cr_2O_3 in the Cr^{3+} - Al^{3+} coupled experiments varied from 20.79 to 21.55 wt% with an Al_2O_3 content of 7.1-7.4 wt%. The Al_2O_3 content in the Al^{3+} only experiments varied from 8.83 to 9.2 wt% and SiO_2 was substituted for the missing Fe_2O_3 and Cr_2O_3 in order to allow the glasses to melt at 1150°C . The as-made compositions are given in Table IV. Glasses were air quenched in their crucibles. In order to study the Fe^{2+} - Fe^{3+} and Fe^{2+} - Cr^{3+} pairs the glasses were made with coal as a reductant and the final $\text{Fe}^{2+}/\Sigma\text{Fe}$ measured [87]. The resulting glasses were analyzed by x-ray diffraction (Table III) and energy dispersive analysis by X-ray (EDAX) during Scanning Electron Microscopy (SEM) for phase identification.

(2) T_L Database Glasses

Approximately 50 glasses designated the Extreme Composition Matrix, representing waste glass extremes in Al_2O_3 and Fe_2O_3 content,* were fabricated at SRNL from reagent grade oxides, carbonates, and hydroxides, in high purity Al_2O_3 crucibles at $1150^\circ C$, the nominal DWPF melt temperature. Due to inherent co-linearity of species in the waste, these glasses represent composition extremes but lack variations amongst individual components. The glasses were made in both reduced and oxidized states spanning $Fe^{+2}/\Sigma Fe$ ratios of 0.01 to 0.47. The glasses were held at the melt temperature for 4 hours, air quenched in the crucible, removed, and analyzed by x-ray diffraction to ensure that the sample was amorphous. The glasses were sent to both Corning Engineering Laboratory Services (CELS)^{††} and Sharp-Shurtz (now Owens Corning Testing) for liquidus temperature (T_L) measurements by ASTM C829 [36] and to CELS for replicate chemical analyses. The T_L values of a subset of 6 glasses, all highly reduced, were measured three to five times by CELS over a 4 year time frame. These same glasses were also analyzed by Pacific Northwest National Laboratory (PNNL) in duplicate using a recently developed isothermal liquidus temperature procedure [35]. When replicate T_L measurements made by the various laboratories were in disagreement, confirmation testing at SRNL was performed using isothermal T_L measurement. Glasses for which spinel was not identified as the primary phase are shaded in Table V and are not used in subsequent modeling.

The compositions of the SRNL glasses whose liquidus temperature measurements are provided in Table V were primarily analyzed by CELS; the compositions for these glasses are also provided in Table V. CELS analyzed most of the glasses in quadruplicate[†] so that any effects of short term instrument bias on the whole element chemistry would be minimized. CELS analyzed the various frits six times. All CELS composition analyses are traceable to the NBS777 standard glass. These data indicate little random or systematic variation for these analyses. Two glasses (AH 168AL-1988 and AH 168FE-RED-1988) were analyzed by the Analytic Development Section (ADS) of SRNL. These samples were prepared using dissolution by either Na_2O_2 with an HCl uptake or HCl/HF/microwave followed by analysis by Inductively Coupled Plasma (ICP) Spectroscopy and Atomic Absorption (AA) [88]. The $Fe^{2+}/\Sigma Fe$ analyses were performed on selected glasses and used to compute the FeO values reported in Table V. For those glasses without $Fe^{2+}/\Sigma Fe$ determinations, glasses that were fabricated without the addition of a reductant, the $Fe^{2+}/\Sigma Fe$ values were assumed to be one-half the detection limit [89] for this measurement, $Fe^{2+}/\Sigma Fe = \frac{1}{2}(0.03) = 0.015$.

A second set of 51 compositions designated as the DWPF Statistically Designed Matrix was designed by SRNL to cover the range of waste glass extremes in Al_2O_3 and Fe_2O_3 . This data set, designated the “SG” glasses, included two glasses which were compositional replicates of each other (i.e., SG05 and SG18). These glasses were made at PNNL from reagent grade chemicals,

* the glasses were fabricated with “waste loadings” calculated on an oxide basis and varying between 25 and 35 wt% for high Fe_2O_3 containing Purex waste, high Al_2O_3 HM waste, and average waste (a mixture of the two).

^{††} ASTM C829 states that a precision of $\pm 10^\circ C$ is achievable for T_L measurement with clear glasses tested in the same furnace. No precision is given for glasses tested in different furnaces or for opaque glasses. CELS provided estimates of $\pm 20^\circ C$ (twice the ASTM value) for black opaque waste glasses.

[†] two dissolutions were performed (one on each day) with each dissolution analyzed in duplicate.

melted for 1 hour in Pt-Rh crucibles, quenched on either a stainless steel plate or into water, ground, remelted, quenched again and reground again before liquidus measurement. Glasses were melted at a variety of temperatures ranging between 1107°C and 1384°C. The compositions were measured by SRNL in duplicate [90]. The details of the glass fabrication and T_L measurement are available elsewhere [91]. The precision of the PNNL isothermal temperature method was reported to be $\pm 12^\circ\text{C}$ for bias-corrected liquidus measurements [91] based on replicate analyses of a waste glass standard (SP-1).[‡] During a subsequent study (designated the SG1 study) that included the effect of variable quench rate, the long term precision of the SP-1 glass was found to be as large as $\pm 30^\circ\text{C}$ [90,91].

The liquidus temperature measurements and compositions for the SG glasses are provided in Table V. Only those SG Study glasses exhibiting spinel[†] whether or not it is in conjunction with clinopyroxene were used for modeling; this eliminates the seven glasses from modeling consideration as indicated by the shading in Table V. This constraint provides 59 measured liquidus temperatures for 44 additional glass compositions were pooled with the SRNL extreme composition study glasses. As with the extreme composition study glasses, the short-term PNNL liquidus temperature measurements from the SG Study were averaged, e.g. the T_L measurements for the SG06(2), SG18(7), SG18B(5), SG25(2), and SG37(2). The seven SG18 and five and SG18B measurements were averaged over the various PNNL furnaces used for heat-treatment into two sets of three values each because the use of different furnaces was believed to have introduced the observed long-term biases. The averaging decreases the unique SG model data to 50 liquidus temperatures for a total modeling population of 105 measurements.

(3) Residual Melt Pool Glass

Varying amounts of acmite and spinel crystallized in a pilot scale melter in the 1980's. The amount of crystallization caused the melt to lose the capacity to sustain Joule heating. The crystals were analyzed by electron microprobe. The residual glass around the crystalline phases was isolated and chemically analyzed by the dissolution methods described above. The here-to-fore unpublished data is presented here to demonstrate how the liquidus model developed in this study applies to volume crystallization in an actual waste glass melter.

IV. RESULTS AND DISCUSSION

(1) Relative Stability of Melt Quasicrystals Vs. Crystalline Liquidus Phases

In order to understand the role of the OSPE and the relative stability of spinel forming quasicrystals $Y_{0.5}AlO_2$, $Y_{0.5}CrO_2$, and $Y_{0.5}FeO_2$ ($Y = Ni^{2+}$, Fe^{2+} , Mn^{2+} and Mg^{2+}) versus the stability of the Y, Al, Cr, and Fe^{3+} cations in crystalline spinels being formed, the divalent cation effects were studied one at a time in the presence and absence of the tetrahedral Al, Cr, and Fe^{3+}

[‡] The SP-1 glass was used by PNNL during the SG Study to correct the liquidus temperature measurements on a furnace to furnace basis by between 1 and 33°C. The accepted value for the SP-1 glass is 1040°C [91]

[†] As in one of the SRNL model data (i.e., one of the DWPF Startup Frit glasses), some of the glasses exhibit both spinel and (clino)pyroxene to the resolution of the liquidus temperature measurement.

species (see Table III and Table IV). Since alkali (X =K, Na, Li) is always present in waste glasses from either the waste or the glass forming frits, these one at a time interactions could be used to qualitatively determine the relative stability of the $Y_{0.5}AlO_2$, $Y_{0.5}CrO_2$, and $Y_{0.5}FeO_2$ in the melt, the $XAlO_2$, $XCrO_2$, and $XFeO_2$ in the melt, and the role of the Y and Al, Cr, and Fe^{3+} cations in the crystalline spinels with which the melt was in equilibrium at typical melt temperatures of $\sim 1150^\circ C$.

In the absence of Al^{3+} and Cr^{3+} in the melt, the spinels that form at melt temperatures between $1050-1150^\circ C$ are $MgFe_2O_4$, $NiFe_2O_4$ and $FeFe_2O_4$ (Table III). While $NiFe_2O_4$ and $FeFe_2O_4$ also form in the combined presence of Fe^{3+} and Al^{3+} in the melt, $MgFe_2O_4$ does not. Likewise, $MgCr_2O_4$ does not form in the combined presence of Cr^{3+} and Al^{3+} in the melt. This indicates that crystalline $MgFe_2O_4$ can only form in the absence of aluminate ($Mg_{0.5}AlO_2$ or $XAlO_2$) or chromate ($Mg_{0.5}CrO_2$ or $XCrO_2$) quasicrystals in the melt. This also indicates that magnesium or alkali $[^4]Fe^{3+}$ quasicrystals ($Mg_{0.5}FeO_2$ or $XFeO_2$) are more stable in the melt than $[^6]Mg^{2+}$, $[^6]Fe^{3+}$, or $[^4]Fe^{3+}$ in crystalline spinel when Al^{3+} and/or Cr^{3+} is present. This is confirmed by the lack of crystallization of $MgFe_2O_4$ or $MgCr_2O_4$ in the melts in which both Fe^{3+} and Al^{3+} are present or Cr^{3+} and Al^{3+} are present. In summary, $Mg_{0.5}AlO_2$ (melt) is more stable in the melt than $Mg_{0.5}FeO_2$ (melt) which in turn is more stable than crystalline $MgFe_2O_4$ or mixed $Mg(Fe,Al)_2O_4$.

$NiFe_2O_4$ and $FeFe_2O_4$ spinels crystallize at melt temperatures of $1050-1150^\circ C$ in the presence or absence of Al^{3+} in the melt indicating that the high OSPE of $[^6]Ni^{2+}$ and $[^6]Fe^{3+}$ in crystalline $NiFe_2O_4$ dominates whether the melt is depleted in $[^4]Al^{3+}$ species such as $XAlO_2$ or not. In comparison, no chromate spinels form in a chromate rich melt when Al^{3+} was absent. This indicates that $[^4]Cr^{3+}$ quasicrystals (such as $XCrO_2$) are more stable in the melt than $[^6]Cr^{3+}$ in the crystalline species. It also indicates that despite the high OSPE of $[^6]Ni^{2+}$ and $[^6]Cr^{3+}$, $NiCr_2O_4$ spinel will not crystallize (maximize the polarization energy of Ni^{2+}) when the melt is depleted in tetrahedral $[^4]Al^{3+}$ so Ni remains tetrahedral as $[^4]Ni^{2+}$ in the melt.

The crystallization of the trevorite ($NiFe_2O_4$) and magnetite ($FeFe_2O_4$) also indicates that the $[^6]Ni^{2+}$ $[^6]Fe^{3+}$ and $[^6]Fe^{2+}$ $[^6]Fe^{3+}$ of the crystalline spinels are more stable than $[^4]Fe^{3+}$ quasicrystals in the melt, e.g. (K,Na,Li) FeO_2 . The absence of the formation of $MgFe_2O_4$ and $MnFe_2O_4$ in the presence of both Fe^{3+} and Al^{3+} in the melt indicates that the $Mg_{0.5}AlO_2$ and $Mn_{0.5}AlO_2$ or $XAlO_2$ and $XFeO_2$ quasicrystals in the melt are more stable than the corresponding ferrite crystalline spinels.

When Cr^{3+} and Al^{3+} are together in a melt, the normal situation in waste glasses, both $NiCr_2O_4$ and $MnCr_2O_4$ readily crystallize. This demonstrates that the Ni^{2+} and Cr^{3+} OSPE energy term dominates when sufficient $[^4]Al^{3+}$ is present in the melt. The crystallization of the chromate spinels also indicates that the $[^6]Ni^{2+}$ $[^6]Cr^{3+}$ and $[^6]Mn^{2+}$ $[^6]Cr^{3+}$ of the crystalline species are more stable than $[^4]Cr$ quasicrystals in the melt. The absence of the formation of $MgCr_2O_4$ and $FeCr_2O_4$ in the presence of both Cr^{3+} and Al^{3+} in the melt indicates that the $Mg_{0.5}AlO_2$ and $Fe_{0.5}AlO_2$ quasicrystals in the melt are more stable than the corresponding chromate crystalline spinels. Lastly, the lack of any spinel formation in Al^{3+} only melts is an indication that all of the $[^4]Al$ quasicrystals in the melt, e.g. $Fe_{0.5}AlO_2$, $Mg_{0.5}AlO_2$, $Mn_{0.5}AlO_2$, $Ni_{0.5}AlO_2$ and/or $XAlO_2$, are more stable than the corresponding $[^6]Al$ positions in crystalline aluminate spinels.

Divalent manganese, the only manganese species present at temperatures >1050°C in waste glasses [92], does not participate in any crystallization in the 1050-1150°C melt temperature range regardless of the presence or absence of Fe³⁺ and Al³⁺. Divalent manganese only crystallizes as MnCr₂O₄ spinel in the presence of Al³⁺ and Cr³⁺. The data in Table III and Table IV demonstrates that the spinels analyzed in nuclear waste glasses are solid solutions of NiFe₂O₄, NiCr₂O₄, and MnCr₂O₄ and may also explain the increase in Cr content in the spinels in Figure 2 with increase in equilibration temperature.

Using this qualitative approach, the data in Table III and Table IV indicate that the OSPE for the formation of spinels in nuclear waste glasses is Ni≈Fe²⁺>Mg²⁺>Mn²⁺ in agreement with the sequences determined in previous studies in simpler systems [39,41]. In addition, the presence of LiCr(SiO₃)₂ as a phase in Table III is an indication that LiCrO₄ in the presence of excess SiO₂ (LiCr(SiO₃)₂ = LiCrO₄ + 2SiO₂) may also be present in nuclear waste glasses as a quasicrystalline species similar to LiFeO₄ and NaFeO₄ quasicrystals observed previously during crucible and pilot scale melter tests [14,23].

It should also be recognized that the melt has a dynamic equilibrium between the aluminate, ferrate, and chromate quasicrystals formed with X and Y cations and the silicate quasicrystals formed with X and Y cations (Equation 2). Strong evidence that the cation Li is primarily present as a silicate quasicrystalline species comes from the ubiquitous formation of Li₂Si₂O₅ as a phase during the determination of all time-temperature-transformation (TTT) diagrams for simulated waste glasses. Since little to no Li substitutes into the nepheline structure (it is too small for the 8-9 coordinated M1 sites in nepheline [47]) it crystallizes out as a separate silicate phase. In the absence of Fe³⁺, Al, Ni, Fe²⁺, Mn²⁺, and Mg from the waste, e.g. the heat treatment of an alkali borosilicate frit (F165) at 700°C for 24 hours, this lithium disilicate phase is the only phase to form. Likewise, a Mn²⁺-Fe³⁺ rich melt (Table III) that was amorphous when held at 1050°C for 4 hours is heat treated for 24 hours, the disilicate Ca(Mn,Ca)Si₂O₆ phase (bustamite) crystallizes. Thus it appears that Ca²⁺, Mn²⁺ and Li⁺ may all be strongly associated with silicate quasicrystals instead of the aluminate, ferrate, or chromate quasicrystals.

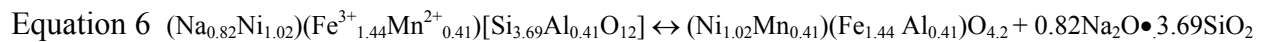
The distribution of the chromate, ferrate, aluminate, and silicate quasicrystalline groups in the melt are temperature dependent but the degree of order (normal spinel vs. inverse spinel structure), which determines the coordination of the trivalent cations in crystalline spinel, is also a strong function of temperature [93]. Therefore, the exchange reactions between ^[4]Cr³⁺_(melt)-^[6]Cr³⁺_(crystal), ^[4]Fe³⁺_(melt)-^[6]Fe³⁺_(crystal), and ^[4]Al³⁺_(melt)-^[6]Al³⁺_(crystal) define the shape of the liquidus in these complex 15 component systems. Since the ferrite spinels like NiFe₂O₄, have an inverse spinel structure, ^[6]Mg²⁺, ^[6]Zn²⁺, ^[6]Fe²⁺, ^[6]Ni²⁺ are in octahedral coordination and half of the Fe³⁺ is in octahedral coordination (^[6]Fe³⁺) while in the chromate and aluminate spinels all the divalent species are tetrahedrally coordinated and ^[6]Cr³⁺ and ^[6]Al³⁺ are octahedrally coordinated [39,40,41], exchange reactions of the following type between the melt species (LHS) and the primary crystalline phases (RHS) are likely:

[32] spinel depending on the availability of Fe^{2+} or other divalent cations, and nepheline (Ne). These include the Ac-Ne-Ds (disilicate) ternary [96], the Ac-Ne-Jd (jadeite) ternary, the Ac-Ne-5:1:8 compound ($5\text{Na}_2\text{O}\bullet\text{Fe}_2\text{O}_3\bullet 8\text{SiO}_2$) ternary, and the Ac-Ne- Fe_2O_3 ternary [31].

The incongruent melting of acmite under oxidizing conditions yields a mixture of crystalline Fe_2O_3 and an alkali silicate liquid (Equation 5), this liquid, is a mixture of alkali disilicate and silica, further justifying the initial use of the Ac-Ne-Ds ternary system as a starting point for the spinel-nepheline liquii.



In addition, Fe_2O_3 has been shown to be a reactive template for the formation of $(\text{Mn,Zn})\text{Fe}_2\text{O}_4$ spinels because the $\langle 111 \rangle$ of the spinel is topotactic with the $\langle 001 \rangle$ of the template Fe_2O_3 phase [97]. Therefore, if melted, the nickel rich acmite found in waste glasses (Table II) could easily act as a template for $(\text{Ni,Mn})\text{Fe}_2\text{O}_4$ spinel and sodium disilicate found on the spinel/acmite liquidus (Equation 6):



The goal of the quasicrystalline spinel-nepheline model was to treat the waste glass melt as an MRO lattice of contrasting degrees of polymerization, e.g. Q^4 (stuffed tridymite like structures) and Q^2 (pyroxene and/or disilicate chain like structures). Therefore, the Ac-Ne-Ds ternary system was used as a starting place. This approach is similar to the MRN model [71] which involves two interlacing “sublattices” that have different degrees of order. Moreover, the number of Q^4 units in a melt, e.g. silica tetrahedra that have not reacted with a metal cation to form a non-bridging oxygen, is related to the thermodynamic activity of SiO_2 in the melt and thus the Q distribution is related to the freezing point depression of a glass [77], i.e. the liquidus.

The quasicrystalline liquidus model in the Ac-Ne-Ds system (see Figure 1) for waste glasses was then constrained based on the crystallochemical coordination and known substitutions of cations in the lattice sites of Ac-Ne-Ds in an attempt to define non-stoichiometric melt precursors that define the spinel-nepheline liquidii. Thus, the composition of the quasicrystalline species involved distributing the constituent components in the molten glass just prior to crystal formation into pyroxene (acmite) type precursors, nepheline type precursors, and disilicate type precursors. Elements in the glass that could occupy tetrahedral sites in crystalline pyroxene were designated MT, the elements that could occupy the pyroxene octahedral sites were designated as M1, and the elements that could occupy the pyroxene VI-VIII coordinated sites were designated as M2 (Table VII) after the conventional nomenclature for the pyroxene structural formula [49, 98]:



where M2 designates a distorted 6 to 8 coordination site and M1 and MT designate regular octahedral and tetrahedral coordination sites, respectively. Conventional mineralogic speciation

was also applied to the tetrahedral nepheline sites (designated T2) and the VIII-IX coordinated sites in nepheline (designated N2) [46], and to the tetrahedral (designated as T3) and VI-VIII coordinated sites in a family of disilicates that are structurally similar to the disilicate end-member diopside [49]. While the entire glass composition must be reduced to quasi-lattice representations of Ne-Ac and a residual phase which will include Ds and excess SiO₂, the liquidus surfaces of interest lie between the Q⁴ (Ne) and Q² (Ac) quasi-lattices in the melt.

(2) Quasicrystalline Freezing Point Depression Model

The addition of a nepheline quasi-lattice (solute) to the primary phase pyroxene (acmite) quasi-lattice (the solvent P) from which spinel precipitates lowers the freezing point, which is equivalent to a change in the solubility of the melt [99]. This condition requires the chemical potentials, μ_P , of the pure crystalline primary phase, P, and of P in the liquid (or melt) to be equal at any point along the freezing point curve. At a given, constant pressure and liquidus temperature, T_L , this means that the potentials are related by [99]:

$$\text{Equation 8} \quad \mu_{P(s)}^*(T_L) = \mu_{P(l)}^*(T_L) + RT_L \ln\{a(P_{(l)})\}$$

where μ is the appropriate chemical potential, $a(P_{(l)})$ represents the activity of P in the liquid (or melt) phase, R is the appropriate gas constant, and the asterisk (*) indicates a pure substance. Rearranging this expression provides:

$$\text{Equation 9} \quad \mu_{P(l)}^*(T_L) - \mu_{P(s)}^*(T_L) = -RT_L \ln\{a(P_{(l)})\}.$$

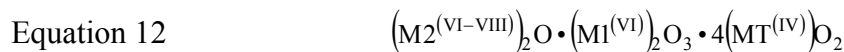
This can be used to provide a relationship between the activity of P in the liquid (or melt) phase and the reciprocal of the liquidus temperature:

$$\text{Equation 10} \quad -R \ln\{a(P_{(l)})\} \approx \Delta\bar{H}_{\text{fus,P}} \left(T_P^* \right) \left(\frac{1}{T_L} - \frac{1}{T_P^*} \right).$$

A relationship similar to Equation 10 is used in the quasicrystalline liquidus model to estimate the liquidus on the binary phase diagram between acmite (spinel) and nepheline. As in ideal solutions, it is assumed that the molar concentration of P may be substituted for the activity of P in Equation 10. The activity of P, the pyroxene quasicrystalline species in the melt for waste glasses (which are not simple binary systems) remains an unknown in Equation 10 and must be approximated. The pyroxene formula from Equation 10 can be represented by:



or



where the cation coordination numbers are provided in superscripts and Equation 12 is on the same oxide formula basis as acmite. Thus for the acmite(spinel)-nepheline binary system represented in Figure 1, the equilibrium activity of pyroxene (P) in the liquid phase (based upon Equation 12) would be proportional to the liquid phase oxide activities raised to their respective stoichiometric coefficients, or:

$$\text{Equation 13} \quad a(P_{(l)}) \propto a((M2)_2O_{(l)})^a a((M1)_2O_{3(l)})^b a((MT)O_{2(l)})^4$$

where the constant of proportionality is represented by the equilibrium constant, K_p , for pyroxene. The liquid phase activity for a component (e.g., $a\{A\}$) can then be expressed as the product of its activity coefficient (e.g., $\gamma\{A\}$) and molar concentration (e.g., $[A]$), or

$$\text{Equation 14} \quad a(P_{(l)}) = K_p \{\gamma((M2)_2O_{(l)})\} [(M2)_2O_{(l)}] \{\gamma((M1)_2O_{3(l)})\} [(M1)_2O_{3(l)}] \{\gamma((MT)O_{2(l)})\} [(MT)O_{2(l)}]^4$$

A number of assumptions and resulting simplifications will be made to Equation 14 to provide as simple a composition basis as possible for defining the pyroxene quasicrystalline species. The initial assumption is that the liquid phase reaction producing pyroxene as described by Equation 14 behaves ideally, that is, all γ 's equal unity[†]. This results in the following approximate relationship for the liquid phase pyroxene activity:

$$\text{Equation 15} \quad a(P_{(l)}) \approx K_p [(M2)_2O_{(l)}]^a [(M1)_2O_{3(l)}]^b [(MT)O_{2(l)}]^4$$

Another assumption is that, because many pyroxenes contain voids, that the stoichiometric ratios of the M2:M1:MT sites in the liquid pyroxene phase are not necessarily in the ratios of 1:1:4. Thus the pyroxene liquid phase activity will be represented by:

$$\text{Equation 16} \quad a(P_{(l)}) \approx K_p [(M2)_2^{(v1)}O_{(l)}]^a [(M1)_2O_{3(l)}]^b [(MT)O_{2(l)}]^c$$

It remains to define the appropriate molar concentrations to allow liquidus temperature to be predicted from the melt composition.

Table VII indicates that various cations (e.g., Fe^{3+} , Al^{3+} , Mg^{2+} , etc.) may occupy multiple sites in pyroxene and it is assumed that the same substitutions can occur in the quasicrystalline melt phase precursor. However, the definition of a reasonable composition basis for liquidus temperature prediction is complicated by the fact that many of these same cations are present in the substituted nepheline precursor and/or disilicate melt phase complex. It is further assumed that this will be the case in the hypothesized melt phase complexes or precursors representing

[†] Alternatively, one could assume that the activity coefficients are constant over the given temperature range. This would be akin to defining a new constant, $K'_p = K_p \gamma_1 \gamma_2 \gamma_3^4$, and proceeding as described. However, for the sake of simplicity, ideal behavior (i.e., unitary activity coefficients) has been assumed.

(substituted) nepheline and general disilicate. This is not to say that the melt phase complexes or precursors have exactly the same structure as their corresponding crystalline analogs (as they likely will not) nor that the cations in the melt phase precursors have the same coordination numbers as in the corresponding crystalline structures; this is merely one way to represent the complicated melt phase complexes. Further, it is assumed that if a cation is associated with a site in one quasicrystalline melt phase complex, it will not be available to another complex or precursor. However, this does not mean that there is not some degree of interchange of cations as crystalline material begins to form at the liquidus temperature (i.e., the system establishes a new equilibrium at the given temperature). The resulting assumed cation distribution information is provided in Table VII.

The availability of cations to the various melt phase complexes or precursors can be accounted for by defining the following molar site distributions based on the information in Table VII:

Pyroxene-like Complex or Precursor:[†]

$$\begin{aligned}\Sigma_{MT} &\equiv \phi_{T, SiO_2} Z_{SiO_2} + \phi_{T, Al_2O_3} Z_{Al_2O_3} + \phi_{T, Fe_2O_3} Z_{Fe_2O_3} \\ \Sigma_{M1} &\equiv \phi_{M1, Al_2O_3} Z_{Al_2O_3} + \phi_{M1, Fe_2O_3} Z_{Fe_2O_3} + \phi_{M1, TiO_2} Z_{TiO_2} + \phi_{M1, Cr_2O_3} Z_{Cr_2O_3} + \phi_{M1, ZrO_2} Z_{ZrO_2} \\ &\quad + \phi_{M1, NiO} Z_{NiO} + \phi_{M1, MgO} Z_{MgO} + \phi_{M1, MnO} Z_{MnO} \\ \Sigma_{M2} &\equiv \phi_{M2, NiO} Z_{NiO} + \phi_{M2, MgO} Z_{MgO} + \phi_{M2, MnO} Z_{MnO} + \phi_{M2, CaO} Z_{CaO} \\ &\quad + \phi_{M2, K_2O} Z_{K_2O} + \phi_{M2, Li_2O} Z_{Li_2O} + \phi_{M2, Na_2O} Z_{Na_2O}\end{aligned}$$

Nepheline-like Complex or Precursor:

$$\begin{aligned}\Sigma_{T1} &\equiv \phi_{T1, SiO_2} Z_{SiO_2} + \phi_{T1, Al_2O_3} Z_{Al_2O_3} + \phi_{T1, Fe_2O_3} Z_{Fe_2O_3} + \phi_{T1, TiO_2} Z_{TiO_2} \\ \Sigma_{N1} &\equiv \phi_{N1, K_2O} Z_{K_2O} + \phi_{N1, Li_2O} Z_{Li_2O} + \phi_{N1, Na_2O} Z_{Na_2O}\end{aligned}$$

where $\phi_{i,j}$ is the fraction of the moles of j associated with the i^{th} site and z_j represents the total moles of j per 100 grams of glass. The manner in which the fractions are defined is discussed below.

Thus the appropriate mole fractions to use in Equation 16 to represent the liquid phase activities for the components comprising the proposed melt phase complexes or precursors are:[†]

$$M_2 = [(M2)_2O_{(l)}] \equiv \frac{\Sigma_{M2}}{\Sigma}, \quad M_1 = [(M1)_2O_{3(l)}] \equiv \frac{\Sigma_{M1}}{\Sigma}, \quad \text{and} \quad M_T = [(MT)O_{2(l)}] \equiv \frac{\Sigma_{MT}}{\Sigma}$$

where

$$\Sigma \equiv \Sigma_{M2} + \Sigma_{M1} + \Sigma_{MT} + \Sigma_{T1} + \Sigma_{N1}$$

because only the pyroxene-nepheline pseudobinary is of concern. The pyroxene melt phase precursor liquid phase activity can then be approximated by:

[†] A term representing the ZnO concentration must be added to Σ_{M2} when the liquidus temperatures of glasses containing significant concentrations of this oxide are to be predicted.

[†] This appears consistent with the concept of site fractions (i.e., the number of atoms in a particular structural site divided by the total number of sites of that type available) that is normally applied to the chemistry of imperfect crystals. For more information, please refer to: F.A. Kroger, **The Chemistry of Imperfect Crystals**, North-Holland Pub. Co., Amsterdam, The Netherlands, 1039 pp. (1964).

Equation 17
$$a(P_{(l)}) \approx K_p (M_2)^a (M_1)^b (M_T)^c$$

and Equation 10 then, upon substitution, becomes:

Equation 18
$$-R \ln \{ K_p (M_2)^a (M_1)^b (M_T)^c \} \approx \Delta \bar{H}_{\text{fus},P} (T_p^*) \left(\frac{1}{T_L} - \frac{1}{T_p^*} \right).$$

Equation 18 provides a relationship between melt concentrations and the liquidus temperature, T_L . Rearranging the above relationship provides a way to estimate the (reciprocal) liquidus temperature as a function of the molar melt constituent concentrations:

Equation 19
$$\left(\frac{1}{T_L} \right) \approx - \frac{R}{\Delta \bar{H}_{\text{fus},P} (T_p^*)} \ln \{ M_2^a M_1^b M_T^c \} + \left\{ \left(\frac{1}{T_p^*} \right) - \frac{R \ln(K_p)}{\Delta \bar{H}_{\text{fus},P} (T_p^*)} \right\}.$$

Equation 19 provides a parsimonious basis for predicting liquidus temperature for waste glasses assuming the presence of a pyroxene intermediate that then melts incongruently to spinel. Thus to a priori predict the liquidus temperatures for a given set of DWPF compositions, the enthalpy of fusion, melt temperature, distribution of cations among melt phase complexes or precursors, and equilibrium constant and stoichiometry of the pertinent equilibrium reaction must be known. In the case of waste glasses, such information is not available; therefore, this information is estimated from fitting available data.

During the fit of Equation 19 to the liquidus data in Table V for the statistically designed data set, the quasicrystalline lattice speciation was constrained based on the known role of each element in the crystalline pyroxene (acmite) and nepheline end members (see coordination of each element given in Table VII). For example, the available Si^{4+} cations (corresponding to moles of SiO_2) were initially distributed equally among the MT, T2, and T3 tetrahedral sites and the Al^{3+} cations (corresponding to the moles of Al_2O_3) were distributed equally among the MT, M1, T2, and N2 sites. Because there are no data on how such cations are distributed in molten glass, a trial-and-error method was used to improve the initial estimates of the cation distributions. In other words, it was hypothesized that the model represented in Equation 19 would be reasonable for the waste glasses in this study and the distribution of the cations were varied systematically (while constrained by the information in Table VII) until the resulting model described the DWPF Statistically Designed Study data with no lack-of-fit. The estimated distributions for this model are provided in Table VIII. Thus if 1) the model in Equation 19 is descriptive and 2) the distributions obtained from the 50 SG Study data (which were designed over the expected DWPF composition region) are reasonable, then the model in Equation 19 using the distribution information in Table VIII would also describe the remaining 55 Extreme Composition Data (and pertinent validation data).

Figure 3 illustrates the least-squares relationship for (reciprocal) liquidus temperature as a function of composition for the pooled 105 model data. This relationship has four fitted parameters and has the form:[†]

$$\text{Equation 20} \quad \frac{1}{T_L(K)_{\text{spinel}}} = -0.000260 \ln(M_2) - 0.000566 \ln(M_1) - 0.000153 \ln(M_T) - 0.00144$$

$$= \ln \left\{ (M_2)^{-0.000260} (M_1)^{-0.000566} (M_T)^{-0.000153} \right\} - 0.00144$$

where the new coefficients were obtained from the multi-linear regression of $(1/T_L)$ as the dependent variable and $\ln(M_2)$, $\ln(M_1)$, and $\ln(M_T)$ as the independent variables based upon the speciation provided in Table VIII and the 105 statistically designed and extreme composition model data given in Table V; the least-squares results are $R^2 = 0.891$ and $s_r = 2.28 \times 10^{-5} \text{K}^{-1}$ for the spinel liquidus model. The details of the modeling are given elsewhere [90].

The model developed to predict spinel liquidus temperature, T_L , from composition can also be defined as:

$$\text{Equation 21} \quad T_L(^{\circ}\text{C})_{\text{spinel}} = \{a \ln(M_2) + b \ln(M_1) + c \ln(M_T) + d\}^{-1} - 273$$

where $a = -0.000260$, $b = -0.000566$, $c = -0.000153$, and $d = -0.00144$

and

$$\begin{aligned} \Sigma_{\text{MT}} &\equiv \phi_{\text{T,SiO}_2} Z_{\text{SiO}_2} + \phi_{\text{T,Al}_2\text{O}_3} Z_{\text{Al}_2\text{O}_3} + \phi_{\text{T,Fe}_2\text{O}_3} Z_{\text{Fe}_2\text{O}_3} \\ \Sigma_{\text{M1}} &\equiv \phi_{\text{M1,Al}_2\text{O}_3} Z_{\text{Al}_2\text{O}_3} + \phi_{\text{M1,Fe}_2\text{O}_3} Z_{\text{Fe}_2\text{O}_3} + \phi_{\text{M1,TiO}_2} Z_{\text{TiO}_2} + \phi_{\text{M1,Cr}_2\text{O}_3} Z_{\text{Cr}_2\text{O}_3} + \phi_{\text{M1,ZrO}_2} Z_{\text{ZrO}_2} \\ &\quad + \phi_{\text{M1,NiO}} Z_{\text{NiO}} + \phi_{\text{M1,MgO}} Z_{\text{MgO}} + \phi_{\text{M1,MnO}} Z_{\text{MnO}} \\ \Sigma_{\text{M2}} &\equiv \phi_{\text{M2,NiO}} Z_{\text{NiO}} + \phi_{\text{M2,MgO}} Z_{\text{MgO}} + \phi_{\text{M2,MnO}} Z_{\text{MnO}} + \phi_{\text{M2,CaO}} Z_{\text{CaO}} \\ &\quad + \phi_{\text{M2,K}_2\text{O}} Z_{\text{K}_2\text{O}} + \phi_{\text{M2,Li}_2\text{O}} Z_{\text{Li}_2\text{O}} + \phi_{\text{M2,Na}_2\text{O}} Z_{\text{Na}_2\text{O}} \\ \Sigma_{\text{T1}} &\equiv \phi_{\text{T1,SiO}_2} Z_{\text{SiO}_2} + \phi_{\text{T1,Al}_2\text{O}_3} Z_{\text{Al}_2\text{O}_3} + \phi_{\text{T1,Fe}_2\text{O}_3} Z_{\text{Fe}_2\text{O}_3} + \phi_{\text{T1,TiO}_2} Z_{\text{TiO}_2} \\ \Sigma_{\text{N1}} &\equiv \phi_{\text{N1,K}_2\text{O}} Z_{\text{K}_2\text{O}} + \phi_{\text{N1,Li}_2\text{O}} Z_{\text{Li}_2\text{O}} + \phi_{\text{N1,Na}_2\text{O}} Z_{\text{Na}_2\text{O}} \end{aligned}$$

and

$$M_2 \equiv \frac{\Sigma_{\text{M2}}}{\Sigma}, M_1 \equiv \frac{\Sigma_{\text{M1}}}{\Sigma}, M_T \equiv \frac{\Sigma_{\text{MT}}}{\Sigma}, \text{ and } \Sigma \equiv \Sigma_{\text{M2}} + \Sigma_{\text{M1}} + \Sigma_{\text{MT}} + \Sigma_{\text{T1}} + \Sigma_{\text{N1}}.$$

The spinel liquidus model is semi-empirical in that the coefficients a , b , c , and d were fit to the data based upon a mathematical representation of the freezing point depression equation. However, relevant waste glass data from West Valley Demonstration Project (WVDP) and Pacific Northwest National Laboratory (PNNL), representing an additional 155 measured liquidus values, confirm that the model given in Equation 20 and Equation 21 adequately predicts liquidus temperatures for waste glasses within the spinel primary phase field for many

[†] Note the logarithmic expansion was used:

$$\ln \{ [M_2^a] [M_1^b] [M_T^c] \} = \ln(M_2^a) + \ln(M_1^b) + \ln(M_T^c) = a \ln(M_2) + b \ln(M_1) + c \ln(M_T).$$

glasses falling outside the model data composition range given in Table VI. The details of the model validation are given elsewhere [90].

The same mathematical representation of the freezing point depression was applied to published nepheline liquidus data by Li, et. al [55]. There were only 20 data points available and the compositions available were as batched rather than as analyzed compositions. Of the 20 data points 3 had to be excluded because other phases were the predominant liquidus phase (other than nepheline), one contained 20 wt% B₂O₃ and was likely phase separated, one contained no B₂O₃ which was considered unrealistic for a borosilicate waste glass, two were in the primary phase field of albite in the NAS system, and one contained 10 wt% CaO. The nepheline liquidus defined by the remaining 12 data points plus 1 data points from Ramsey [100] (nepheline measured by CELS), one data point from Jantzen and Bickford [22] (TTT diagram construction), and one data point from a TTT curve of the SRNL WCP High Fe glass (Purex) [37] to make a model data set of 15 observations:

$$\text{Equation 22} \quad T_L(^{\circ}\text{C})_{\text{nepheline}} = \{a \ln(N_1) + b \ln(T_1) + c\}^{-1} - 273$$

where $a = -0.0001498$, $b = +0.0005328$, and $c = +0.001757$

and $N_1 \equiv \frac{\Sigma_{N1}}{\Sigma}$, $T_1 \equiv \frac{\Sigma_{T1}}{\Sigma}$, and $\Sigma \equiv \Sigma_{M2} + \Sigma_{M1} + \Sigma_{MT} + \Sigma_{T1} + \Sigma_{N1}$.

$$\begin{aligned} \text{Equation 23} \quad \frac{1}{T_L(\text{K})_{\text{nepheline}}} &= -0.000150 \ln(N_1) + 0.0005328 \ln(T_1) + 0.001757 \\ &= \ln\left\{(N_1)^{-0.000150} (T_1)^{+0.0005328}\right\} + 0.001757 \end{aligned}$$

with an $R^2 = 0.78$. While better data is needed to define the nepheline liquidus more accurately, this is sufficient to illustrate how this data can be used to define the binary phase diagram between spinel and nepheline.

(3) Quasicrystalline Species Calculated from the Liquidus Data and Experimental Verification

The mathematical application of the freezing point depression based on the known speciation of cations in crystalline pyroxene and nepheline lattices (Table VII) to the 105 liquidus data in Table IV generated the quasicrystalline melt precursors given in Table VIII. The pyroxene melt precursor is Al₂O₃ rich containing 100% of the Al₂O₃ and only 12.72% of the Fe₂O₃. In addition the pyroxene precursor contains 92% of the Cr₂O₃, 100% of the MnO, and 10.79% of the NiO which are all spinel formers. The pyroxene end member also contains 64.57% of the 300% M₂O (where M=K, Na, Li). The nepheline precursor contains ~61% of the Fe₂O₃, 46% of the 300% M₂O and no Al₂O₃. The nepheline precursor also contains >50% of the TiO₂ which may explain why TiO₂ so readily nucleates nepheline preferentially [48].

the Ds component must be an Fe₂O₃ rich disilicate. As shown, the model data fall along a tie line between iron-free nepheline and iron-rich acmite. The data used in modeling is plotted along with the Li et. al [55] nepheline data and waste glass data from WVDP. A comparison of Figure 4 and Figure 5 indicates that there is more error associated with the nepheline liquidus than the spinel liquidus model. This is anticipated as the nepheline data set is only 15 data points and most are not analyzed compositions while the spinel liquidus is 105 data points with many replicates in both the measured liquidus and the measured compositions (see Table V).

(4) Construction of the Spinel-Nepheline Pseudobinary System

The correlation of the measured spinel liquidus temperature (°C) vs. Equation 21 (the spinel liquidus model derived in this study) is given in Figure 6 (top) and the correlation of the measured nepheline liquidus temperature (°C) vs. Equation 22 (the nepheline liquidus model derived in this study) is given in Figure 6 (bottom). Once the phase relations in the pseudoternary (Figure 5) were understood and the individual binary liquidus boundaries defined (Figure 6), the pseudobinary phase diagram between the end member nepheline and acmite precursors could be constructed. By calculating the position of the pyroxene precursor in terms of Equation 22, e.g. a value of 0.34 the correct position of the nepheline liquidus on the pseudobinary could be established. By calculating the position of the nepheline precursor in terms of Equation 21, the correct position of the spinel liquidus could be established, e.g. a value of 0. This put the pseudobinary eutectic at a value of 0.64 when calculated in terms of either equation.

Figure 7 shows the pseudobinary diagram between acmite and spinel expressed in terms of the pyroxene and nepheline precursor compositions (mol%) given in Table VIII. The liquidus curves are fit to the measured liquidus data with Equation 21 and Equation 22 in order to generate the logarithmic fit (curvature) of the liquidus surfaces. Pure end member compositions are fit in terms of the pyroxene and nepheline precursor compositions. During modeling, the sum of precursor pyroxene + nepheline terms were constrained to 1 in order to generate a linear binary liquidus surface. Equation 21 and Equation 22 are logarithmically related to the sum of the pyroxene precursor terms and the sum of the nepheline precursor terms, respectively. Therefore, the end member compositions and several phase pure compositions are shown on Figure 7 for reference, and electron microprobe compositions of various spinels, acmites and iron rich nepheline phases from Table II are shown in terms of the pyroxene precursor composition given in Table VIII (un-normalized mole%) adjusted for the contribution of excess iron available in the liquid phase, e.g. the fact that the pseudobinary modeled is not parallel to the acmite-nepheline boundary in the acmite-nepheline-Fe₂O₃ pseudoternary shown in Figure 5.

The nepheline liquidus appears to persist metastably below the eutectic between acmite and spinel as shown in Figure 5. It is interesting to note that the iron rich nepheline analyzed by Li et. al.[44] falls along the nepheline liquidus defined and the oxidized spinel analyzed by Bickford and Jantzen [22] falls along the spinel liquidus boundaries defined in Figure 7. The remainder of the diagram is inferred from the compositions of the analyzed acmites and pyroxenes from Table II and phase pure acmite. All of the phase fields below the acmite-spinel peritectic and the acmite-nepheline eutectic are in equilibrium with Li₂SiO₃ a metasilicate since the liquid is

supersaturated with this phase. This is the major metasilicate phase observed during TTT diagram testing (Section V.6).

(5) Relationship of the Pseudobinary to Melt Pool Volume Crystallization

A pilot scale melter at SRNL known as the Small Cylindrical Melter (SCM) underwent volume crystallization during the second glass melting campaign (SCM-2, 14). The residual composition of the glass found in the melter is given in Table IX and is plotted in Figure 7. Assuming a melt pool temperature of 1150°C puts the composition of this glass right on the spinel liquidus boundary defined by Equation 21 in Figure 7. Assuming further that the melt pool cooled to 1050°C before spinel crystallization began (an undercooling of ~100°C) also puts the composition of the crystallizing spinel determined from microprobe analysis (Table II) on the liquidus boundary defined by Equation 21. Lastly, the acmite that crystallized at lower temperatures, after the melt pool had cooled considerably has a composition (Table II) similar to that of the residual melt pool glass. This data demonstrates that the spinel liquidus modeled in this study is the internal liquidus representative of volume crystallization in a waste glass melter.

(6) Relationship of the Pseudobinary to Time-Temperature-Transformation (TTT) Diagrams

Validation of the spinel liquidus model developed against other laboratory liquidus measurement data sets is given elsewhere [90]. However, validation of the pseudobinary phase diagram given in Figure 7 is validated against the phase assemblages determined in various time-temperature-transformation studies [21,22,37,101]. In general, there is good agreement between the phase diagram generated in Figure 7 from Equation 21 and Equation 22 and the compositional data in Table II and the phases determined to crystallize at various temperatures during the TTT diagram studies as shown in Figure 8.

During isothermal liquidus measurement for the designed spinel data set in Table V, the phase boundary was determined by quenching, crushing the samples and reheating at a given isothermal annealing temperature, e.g. approaching the liquidus from a lower temperature. When glass-forming materials are undercooled into the glassy state and then reheated in this manner to an annealing temperature T which lies between the glass transformation temperature (T_g) and the melt temperature (T_m), copious crystallization is frequently observed [102]. In contrast, when a sample of the same glass is undercooled directly to the annealing temperature, T , from a temperature $>T_m$, the sample may remain free of crystallization for an extended period. The origin of this difference is associated with nuclei which form during cooling and reheating in the first type of heat treatment. This nucleation can be homogeneous or heterogeneous [102]. Measurement of liquidus temperature by gradient furnace measurements avoids the undercooling issue since the sample spans a range of temperatures (liquidus measurement used for the extreme composition matrix in Table V). Several isothermal runs were reversed and the combined isothermal and gradient furnace data sets were modeled to minimize the metastable appearance of phases below their liquidus boundaries, e.g. in the Ostwald-Miers area of undercooling [103]. However, during TTT diagram representation, which is performed by isothermal annealing, the liquidus and solidus phase boundaries were only approached from $>T_m$ [21,22,37,38,42].

Therefore, some discrepancies between the liquidus measurements and the TTT diagram determination of the liquidus boundary are anticipated as shown in Figure 8.

The cooling method by which the nepheline liquidus was approached for the Hanford Envelope D glass is unknown [101]. The TTT crystallization sequences for glasses Hanford Envelope D [101] glass, the SRNL 131 high Al glass [21,22], and the Waste Compliance Plan (WCP) Purex glass [37,38] have the poorest fit to the pseudobinary phase diagram as shown in Figure 8. They are all in or near the eutectic between acmite and nepheline. This region is just below the last spinel liquidus data point modeled, and below the region between the spinel-acmite peritectic. This is the region in which “constitutional undercooling,” which is composition driven rather than temperature driven, can occur [104]. The data for these three glasses suggests that the nepheline liquidus should be steeper (see dotted nepheline liquidus in Figure 8). If better data were available for the nepheline liquidus and for the small composition region that the proposed acmite only liquidus covers, then these discrepancies could be better understood.

(7) Relationship of the Pseudobinary to Melt Polymerization

While the primary phases found on the liquidus surfaces of most glasses is either spinel or nepheline, there are a number of clinopyroxenes (disilicates) or orthopyroxene (metasilicate) phases found as either liquidus phases or in conjunction with spinel crystallization (Table I). In addition, subsolidus phases such as LiSiO_3 (metasilicate) and $\text{Li}_2\text{Si}_2\text{O}_5$ (disilicates) readily form from the residual eutectic melt.

In order to understand the role of melt polymerization in terms of Q^n distribution theory which treats difference in the reactivity of the n non-bridging oxygens (NBO's), one must also examine the role of the alkali metasilicate and alkali disilicates components of the waste glass melts in addition to the nepheline and acmite components related to the crystallization of spinel and nepheline as liquidus phases. Alkali metasilicates are known to form Q^3 sheets while disilicates are known to form mostly Q^2 chains [105,106,107,108]. Nepheline is a Q^4 framework crystalline species [61,77] while pyroxenes like diopside ($\text{CaMgSi}_2\text{O}_6$) and acmite ($\text{NaFeSi}_2\text{O}_6$) are Q^2 clinopyroxene chain structures [61,77]. Diopside (a Ca-Mg pyroxene) glass was also found to contain ~67% Q^2 and 15% Q^4 with no Q^3 groupings and small quantities of Q^0 and Q^1 [108].

In order to relate the phase assemblages formed on the liquidus in the Ac-Ne- Fe_2O_3 system to the presence of excess metasilicate and disilicate in the melt, the ternary representation of Ellison and Navrotsky [79], previously used by these authors to describe HLW glasses, was adopted. This representation involves a ternary phase diagram that represents the structure of the melt rather than stoichiometric end members, e.g. molar $(\text{K,Na,Li})(\text{Al,Fe,Cr})\text{O}_2$ melt tetrahedra, molar SiO_2 , and molar excess alkali, alkaline earth, titania, zirconia, etc. over that associated with the melt tetrahedra.

The Ellison and Navrotsky's [79] structural representation was modified slightly by normalizing the molar compositions to a B_2O_3 free basis because B_2O_3 is of little significance in liquidus crystallization and glasses with >12 wt% B_2O_3 were determined to inhibit pyroxene crystallization [28]. This modified structural representation was applied to the following data:

between the melt polymerization in terms of Q^n distribution theory, e.g. the difference in the reactivity of the n non-bridging oxygens, and the phases that crystallize. On a boron free basis, waste glasses containing $SiO_2(m) < 50\%$ will crystallize nepheline on the liquidus. When a waste glass falls in the Q^3 region of the ternary polymerization diagram, spinel only will crystallize on the liquidus, and when a waste glass composition falls in the Q^2 region spinel and/or pyroxene will crystallize on the liquidus. The more SiO_2 in the melt and the smaller the $(K,Na,Li)(Al,Fe,Cr)O_2$ component of the melt, the more likely the composition is to form only pyroxene on the liquidus instead of a mixture of spinel and pyroxene. This is in agreement with previous findings that high SiO_2 content in a waste glass stabilizes orthopyroxene phases on the liquidus. More Q^3 polymerization in the glass in the presence of excess Fe_2O_3 stabilizes spinel crystallization. This quasicrystalline liquidus model has been used to prevent unwanted crystallization in the world's largest high level waste (HLW) melter for the past three years while allowing 5-10 wt% higher waste loadings to be processed.

ACKNOWLEDGEMENTS

The authors would like to thank Hong Li of PPG Industries (formerly of PNNL) for his unpublished nepheline microprobe data which was key in the determination of nepheline-acmite pseudobinary phase diagram. The authors would also like to acknowledge the helpful suggestions of Dr. Wayne Burnham of University of Arizona and the in depth discussions with Dr. Gordon E. Brown of Stanford University about quasicrystalline melt theory and modeling. Lastly, the authors would like to thank our colleagues at the Pacific Northwest National Laboratory, primarily John D. Vienna, Pavel Hrma and Mike Schweiger. The authors would also like to acknowledge the reviews performed by colleagues at the Savannah River National Laboratory, primarily David K. Peeler and James C. Marra. This research was sponsored by the Department of Energy (EM-50), the Mixed Waste Focus Area (MWFA), the Tanks Focus Area (TFA), and the Savannah River Defense Waste Processing Facility (DWPF) in connection with work done under Contract No. DE-AC09-96SR18500 with the U.S. Department of Energy. Funding for external publication was provided by the Savannah River National Laboratory sabbatical program.

Table I Primary Liquidus Phases Formed at 24 Hours in Simulated Waste Glasses

NUMBER OF GLASSES	WASTE TYPE	PRIMARY LIQUIDUS PHASE(S)	GLASS CHEMISTRY	REF.
51	DWPF-Average, High Al ₂ O ₃ , + High Fe ₂ O ₃	50 Spinel 1 Nepheline	Frits 165, 131 for sludge only flowsheet, Frits 200, 202 for coupled waste flowsheet, DWPF Startup Frit	This study
1	None	Tridymite + Unknown	Pure Frit 165	This study
2	DWPF-Average	Spinel	2.8 wt% UO ₂ , 0.26 wt% ThO ₂ , noble metals, Frit 165, Fe ²⁺ /ΣFe = 0.01 to 0.21 ± 0.02	42
1	DWPF-High Al ₂ O ₃	Spinel + Nepheline	0.91 wt% UO ₂ , 1.08 wt% ThO ₂ , noble metals, Frit 131, a high Na ₂ O frit with TiO ₂ which may help nucleate nepheline.	22
1	DWPF-High Al ₂ O ₃	Spinel	0.91 wt% UO ₂ , 1.08 wt% ThO ₂ , Frit 165, noble metals	22
2	DWPF-Average	Spinel	2.27 wt% UO ₂ , 0.29 wt% ThO ₂ , Frits 131/165, noble metals	22
2	DWPF-High Fe ₂ O ₃	Spinel	4.15 wt% UO ₂ , 0.03 wt% ThO ₂ , Frits 131/165, noble metals	22
1	DWPF-High Al ₂ O ₃	Nepheline	Frit 411, a high Na ₂ O frit	109,110
1	DWPF-High Fe ₂ O ₃	Spinel	Frit 411, frit higher in Li ₂ O and lower Na ₂ O than Frit 211	109,110
1	DWPF-High Fe ₂ O ₃	Spinel	Frit 211, frit contains more Na ₂ O and less Li ₂ O than Frit 411	109,110
7	DWPF-Average, High Al ₂ O ₃ , + High Fe ₂ O ₃	Spinel	Waste Compliance Plan Glasses (Frit 200+202), noble metals	37,38
24	WVNS	Spinel	Simulated with high ZrO ₂ , non-radioactive	111
3	WVNS	Spinel	0.47 wt% UO ₂ , 3.57 wt% ThO ₂ , noble metals, Fe ²⁺ /ΣFe = 0.1	51,52, 112
33	Hanford HLW Tank Waste - High Fe ₂ O ₃	Spinel	SP glass matrix, noble metals	113
36	Hanford TRU Waste - High ZrO ₂	ZrSiO ₄ , ZrO ₂ , CeO ₂	TRU glass matrix	53
20	Hanford HLW - High Na ₂ O waste	4 Nepheline; 2 Other silicates; 20 Spinel	NP glass matrix; evidence that nepheline grew on spinel crystals	44
51	DWPF-Average, DWPF-High Fe ₂ O ₃ , + DWPF-High Fe ₂ O ₃	44 Spinel 7 Clinopyroxene	SG Glass Matrix, contained noble metals, some glasses contained UO ₂	29
1	Hanford HLW Envelope D Waste	Nepheline + Spinel	Contained noble metals, low SiO ₂ , high Al ₂ O ₃ , high Na ₂ O, and 1.87 wt% UO ₂	101
23	Hanford HLW	11 Spinel; 3 zirconates; 2 Ca-silicate, 2 olivine, 2 SiO ₂ , 1 orthopyroxene	CVS-I, 2 glasses never crystallized	28
100	Hanford HLW	42 Spinel; 4 SiO ₂ , 14 zirconates; 4 Ca-silicate; 2 olivine; 3 orthopyroxene; 10 clino-pyroxene; 6 nepheline; 4 Cr ₂ O ₃ ; 5 LiSiO ₃	CVS-II, contained noble metals, 2 glasses contained UO ₂ and were not measured, 4 glasses did not crystallize	28

Table II Microprobe Analyses of Crystalline Phases in Waste Glasses

GLASS	PHASE (NOMINAL COMPOSITION) [40,46,49]	ANALYZED COMPOSITION	EQUILIBRATION TEMPERATURE (°C)	PRIMARY LIQUIDUS PHASE	REF.
165TDS-U (oxidized)	Spinel, NiFe ₂ O ₄	(Ni _{0.85} Mn _{0.15})(Fe _{0.80} Cr _{0.20}) ₂ O ₄	1003	Yes	42
165TDS-U (reduced)	Spinel, NiFe ₂ O ₄	(Ni _{0.95} Mn _{0.05})(Fe _{0.92} Cr _{0.08}) ₂ O ₄	975	Yes	42
SCM-2	Spinel, NiFe ₂ O ₄	(Ni _{0.77} Mn _{0.31} Mg _{0.02})(Fe _{0.95} Cr _{0.015} Al _{0.003} Ti _{0.002}) ₂ O ₄	Unknown	Yes	This study
SS-A	Spinel, NiFe ₂ O ₄	(Ni _{0.80} Mn _{0.03} Mg _{0.06})(Fe _{0.71} Cr _{0.255} Al _{0.2} Si _{0.2}) ₂ O ₄	Unknown	Yes	29
SP-Si-1	Spinel, NiFe ₂ O ₄	(Ni _{0.62} Mn _{0.07} Mg _{0.31})(Fe _{0.91} Cr _{0.09}) ₂ O ₄ [†]	1101	Yes	43
SP-1	Spinel, NiFe ₂ O ₄	(Ni _{0.74} Mn _{0.05} Mg _{0.21})(Fe _{0.77} Cr _{0.23}) ₂ O ₄ [†]	997	Yes	43
SP-Si-3	Spinel, NiFe ₂ O ₄	(Ni _{0.53} Mn _{0.05} Mg _{0.42})(Fe _{0.31} Cr _{0.69}) ₂ O ₄ [†]	1010	Yes	43
NP-BL	Nepheline, Na ₂ Al ₂ Si ₂ O ₈	(K _{0.02} Na _{1.12} □ _{0.86})[Al _{1.48} Si _{2.14} Fe _{0.24}] ₈ ^{††}	873	Yes	114
SG02 GLASS (Avg. of 4 analyses)	Clinopyroxene in solid solution series acmite-augite (Na ₂ Fe ₂ [Si ₄ O ₁₂]- (Na,Ca) ₂ (Mg,Fe ³⁺ ,Fe ²⁺ ,Al) ₂ [Si ₄ O ₁₂])	(Na _{0.66} Ca _{0.8} Ni _{0.4})(Fe ³⁺ _{1.02} Mg _{0.64} Mn ²⁺ _{0.10} Cr _{0.04})[Si _{4.06} O ₁₂] [†]	775	Yes	29
165TDS-U (reduced)	Acmite, Na ₂ Fe ₂ [Si ₄ O ₁₂]	(Na _{0.82} Ni _{1.02})(Fe ³⁺ _{1.44} Mn ²⁺ _{0.41})[Si _{3.69} Al _{0.41} O ₁₂] [†]	<800	No	42
SCM-2	Acmite, Na ₂ Fe ₂ [Si ₄ O ₁₂]	(Na _{0.74} Ca _{0.96} Ni _{0.04})(Fe ³⁺ _{2.43} Mn ²⁺ _{0.41} Ti _{0.06})[Si _{3.06} Al _{0.06} O ₁₂]	Unknown	No	This study

[†] calculated from data provided in reference so that all spinels were calculated in a consistent manner

^{††} where □ denotes a vacancy

Table III Spinel Solid Solutions Formed in Limited Component Waste Glasses Melted at 1050°C and 1150°C

Only Divalent Cation Present	Fe ³⁺	Fe ³⁺ and Al ³⁺	Cr ³⁺	Cr ³⁺ and Al ³⁺	Al ³⁺
Melt Temperature of 1150°C					
Ni ²⁺	Amorphous	NiFe ₂ O ₄	Cr ₂ O ₃ + SiO ₂	NiCr ₂ O ₄ + Cr ₂ O ₃	Amorphous
Fe ²⁺	Amorphous	Fe ₃ O ₄ *	(Oxidized and reduced) Cr ₂ O ₃ + SiO ₂ Crist [§]	(Oxidized and reduced) Cr ₂ O ₃ [§]	Amorphous ^{§§}
Mn ²⁺	Amorphous	Fe ₂ O ₃ + SiO ₂ (Qtz.)	Cr ₂ O ₃	MnCr ₂ O ₄ + Cr ₂ O ₃	Amorphous
Mg ²⁺	MgFe ₂ O ₄ -Fe ₃ O ₄ Solid solution (poorly crystallized)	Fe ₂ O ₃	Cr ₂ O ₃ + SiO ₂ Crist.	Cr ₂ O ₃	Amorphous
Melt Temperature of 1050°C					
Ni ²⁺	NiFe ₂ O ₄	NiFe ₂ O ₄	Cr ₂ O ₃ + SiO ₂ (Tridy+Crist+Qtz) LiCr(SiO ₃) ₂	Cr ₂ O ₃	SiO ₂
Fe ²⁺	Fe ₃ O ₄ **	Fe ₃ O ₄ *	(oxidized) Cr ₂ O ₃ +LiCr(SiO ₃) ₂ + SiO ₂ Crist (reduced) Cr ₂ O ₃ +LiCr(SiO ₃) ₂ +SiO ₂ (Crist) [§]	(oxidized) Cr ₂ O ₃ +LiCr(SiO ₃) ₂ (reduced)Cr ₂ O ₃ [§]	SiO ₂ ^{§§}
Mn ²⁺	Amorphous	Did not melt	Cr ₂ O ₃	Mn _{1.5} Cr _{1.5} O ₄ + Cr ₂ O ₃	SiO ₂
Mg ²⁺	Amorphous	Fe ₂ O ₃	Cr ₂ O ₃	Cr ₂ O ₃	SiO ₂

* forms at Fe²⁺/ΣFe of 0.1-0.18; otherwise forms Fe₂O₃ at Fe²⁺/ΣFe of 0.02-0.04

** forms at Fe²⁺/ΣFe of 0.1-0.18; otherwise forms Fe₂O₃ at Fe²⁺/ΣFe of 0.02-0.04

§ Since only 2.06-2.22 wt% FeO was theoretically present in these glasses and no Fe₂O₃, the redox measurement is difficult to perform due to excess matrix effects; the redox values designated as reduced were Fe²⁺/ΣFe = 0.02-0.07 so not all of the Fe²⁺ may have been in the reduced state while those designated as oxidized were Fe²⁺/ΣFe = 0-0.05.

§§ Since only 2.58 wt% FeO was theoretically present in these glasses and no Fe₂O₃, the redox measurement is difficult to perform due to excess matrix effects; the Fe²⁺/ΣFe = 0-0.03 so not all the Fe₂O₃ may have been reduced

Table IV Quasi-Chemical Glass Compositions (wt% as-batched)

Oxide Wt. %	NiFe with Al	NiFe w/o Al	MnFe with Al	MnFe w/o Al	MgFe with Al	MgFe w/o Al	FeFe with Al	FeFe w/o Al	NiCr with Al	NiCr w/o Al	MnCr with Al	MnCr w/o Al	MgCr with Al	MgCr w/o Al	FeCr with Al	FeCr w/o Al	NiAl w/o Fe/Cr	MnAl w/o Fe/Cr	MgAl w/o Fe/Cr	FeAl w/o Fe/Cr
Al ₂ O ₃	7.37	0.00	7.17	0.00	7.12	0.00	7.52	0.00	7.37	0.00	7.17	0.00	7.12	0.00	7.34	0.00	9.21	8.90	8.83	9.17
B ₂ O ₃	7.59	8.20	7.39	7.96	7.34	7.90	7.74	8.37	7.59	8.20	7.39	7.96	7.34	7.90	7.57	8.16	9.48	9.18	9.10	9.44
Cr ₂ O ₃	0.00	0.00	0.00	0.00	0.00	0.00	0.00	0.00	19.97	21.55	19.44	20.95	19.31	20.79	19.90	21.48	0.00	0.00	0.00	0.00
Fe ₂ O ₃	19.97	21.55	19.44	20.95	19.31	20.79	18.02	19.49	0.00	0.00	0.00	0.00	0.00	0.00	0.00	0.00	0.00	0.00	0.00	0.00
FeO	0.00	0.00	0.00	0.00	0.00	0.00	2.11	2.28	0.00	0.00	0.00	0.00	0.00	0.00	2.06	2.22	0.00	0.00	0.00	2.58
K ₂ O	3.26	3.52	3.18	3.42	3.15	3.39	3.33	3.60	3.26	3.52	3.18	3.42	3.15	3.39	3.25	3.51	4.08	3.95	3.91	4.06
Li ₂ O	4.51	4.87	4.39	4.73	4.36	4.69	4.60	4.97	4.51	4.87	4.39	4.73	4.36	4.69	4.49	4.85	5.64	5.45	5.40	5.61
MgO	0.00	0.00	0.00	0.00	4.98	5.36	0.00	0.00	0.00	0.00	0.00	0.00	4.98	5.36	0.00	0.00	0.00	0.00	6.17	0.00
MnO	0.00	0.00	4.31	4.65	0.00	0.00	0.00	0.00	0.00	0.00	4.31	4.65	0.00	0.00	0.00	0.00	0.00	5.35	0.00	0.00
Na ₂ O	5.98	6.45	5.82	6.27	5.78	6.22	6.10	6.59	5.98	6.45	5.82	6.27	5.78	6.22	5.96	6.43	7.47	7.23	7.17	7.44
NiO	1.73	1.87	0.00	0.00	0.00	0.00	0.00	0.00	1.73	1.87	0.00	0.00	0.00	0.00	0.00	0.00	2.16	0.00	0.00	0.00
SiO ₂	49.60	53.54	48.29	52.02	47.95	51.63	50.58	54.69	49.60	53.54	48.29	52.02	47.95	51.63	49.42	53.34	61.96	59.94	59.42	61.70
SUM	100.00	100.00	100.00	100.00	100.00	100.00	100.00	100.00	100.00	100.00	100.00	100.00	100.00	100.00	100.00	100.00	100.00	100.00	100.00	100.00

Table V Liquidus Temperature and Measured Composition Data (wt%)†

Sample ID	Year Melted	T _L (°C)	Phases	T _L Reference	Chemical Analysis Replicates	Chemistry Reference ††	Al ₂ O ₃	B ₂ O ₃	CaO	Cr ₂ O ₃	FeO	Fe ₂ O ₃	K ₂ O	Li ₂ O	MgO	MnO	Na ₂ O	NiO	SiO ₂	TiO ₂	Others
DWPF EXTREME COMPOSITION MATRIX																					
AH 131AL	1988	863	S	SS	4	CELS-158	14.05	11.35	0.39	0.002	0.13	3.99	0.05	4.19	1.42	2.69	14.90	0.61	44.60	0.77	0.75
AH 131AL	1992	835	S	CELS-044	4	CELS-044	13.50	10.90	0.38	0	0.09	4.58	0.00	4.09	1.38	2.51	14.10	0.63	46.40	0.72	0.70
AH 131AV	1985	990	S	CELS-009	6	CELS-025	7.18	10.88	0.74	0.074	0.27	11.40	0.04	3.88	1.28	0.82	14.30	1.08	45.20	0.70	0.38
AH 131AV	1992	995	S	CELS-044	4	CELS-044	4.39	7.60	0.76	0	0.29	11.57	0.00	4.25	0.67	2.59	9.86	1.04	54.99	0.06	0.88
AH 131 FE-RED	1992	1075	S	CELS-044	4	CELS-044	2.25	7.33	1.01	0	5.86	11.09	0.00	4.09	0.66	0.93	10.90	2.56	51.40	0.05	0.87
AH 131 FE-RED	1992	1035	S	CELS-076	4	CELS-044	2.25	7.33	1.01	0	5.86	11.09	0.00	4.09	0.66	0.93	10.90	2.56	51.40	0.05	0.87
AH 131 FE-RED	1992	1108	S	PNNL-avg	4	CELS-044	2.25	7.33	1.01	0	5.86	11.09	0.00	4.09	0.66	0.93	10.90	2.56	51.40	0.05	0.87
AH 165AL	1985	863	S	CELS-009	1	CELS-158	13.30	7.57	0.52	0	0.04	4.12	0.05	4.28	0.67	2.75	11.10	0.57	52.70	0.06	1.27
AH 165AL	1992	840	S	CELS-044	4	CELS-044	13.40	7.34	0.51	0	0.12	4.70	0.00	4.20	0.66	2.62	10.60	0.67	53.60	0.00	0.79
AH 165AV	1985	917	S	CELS-009	1	CELS-025	5.34	7.33	0.69	0.052	0.20	11.88	0.06	5.11	0.73	2.78	10.30	1.07	53.10	0.17	0.74
AH 165AV-REV.	1988	1006	S	CELS Letter (5-3-89)	2	CELS-025 CELS-158	5.08	7.27	0.88	0.027	0.20	11.78	0.09	5.09	0.69	2.76	10.23	1.02	53.27	0.11	0.83
AH 165AV	1992	1000	S	CELS-044	4	CELS-044	5.17	6.57	1.04	0	0.19	11.38	0.00	5.02	0.66	2.57	9.96	1.01	55.29	0.00	0.76
AH 165FE-RED	1985	1102	S	CELS-009	1	CELS-158	1.28	7.48	1.49	0.01	6.65	9.71	0.03	4.18	0.66	1.13	11.20	3.05	51.70	0.06	1.26
AH 165FE-RED	1992	1085	S	CELS-044	4	CELS-044	1.42	7.28	1.40	0	5.46	10.93	0.00	4.05	0.65	1.07	10.70	2.97	52.00	0.00	0.85
AH 165 FE-RED	1992	1015	S	CELS-076	4	CELS-044	1.42	7.28	1.40	0	5.46	10.93	0.00	4.05	0.65	1.07	10.70	2.97	52.00	0.00	0.85
AH 165 FE-RED	1992	1100	S	PNNL-avg	4	CELS-044	1.42	7.28	1.40	0	5.46	10.93	0.00	4.05	0.65	1.07	10.70	2.97	52.00	0.00	0.85
AH 165FE-OX	1996	1135	S	CELS-068	4	CELS-068	1.45	7.36	1.42	0	5.99	10.54	0.03	4.27	0.64	1.01	11.20	2.58	49.60	0.00	0.88
AH 168AL	1988	846	S	CELS-022	1	SRNL/ADS	14.16	12.11	0.44	0.001	0.02	3.43	0.23	4.24	0.71	2.66	10.42	0.53	47.66	0.05	0.68
AH 168AV	1985	1014	S	CELS-009	1	CELS-158	5.31	12.65	0.70	0.002	0.63	10.90	0.05	4.28	0.73	2.72	10.30	0.98	50.40	0.06	0.79
AH 168AV	1988	925	S	CELS-022	1	CELS-158	5.31	12.65	0.70	0.002	0.63	10.90	0.05	4.28	0.73	2.72	10.30	0.98	50.40	0.06	0.79
AH 168AV	1992	990	S	CELS-044	4	CELS-044	5.58	10.60	0.68	0	0.61	10.51	0.00	4.24	0.74	2.64	10.10	1.02	51.60	0.00	0.69
AH 168AV	1992	980	S	CELS-076	4	CELS-044	5.58	10.60	0.68	0	0.61	10.51	0.00	4.24	0.74	2.64	10.10	1.02	51.60	0.00	0.69
AH 168AV	1992	969	S	PNNL-avg	1	CELS-044	5.31	12.65	0.70	0.002	0.63	10.90	0.05	4.28	0.73	2.72	10.30	0.98	50.40	0.06	0.79
AH 168FE-RED	1988	1022	S	CELS-022	1	SRNL/ADS	1.44	11.73	1.05	0.014	5.20	7.85	0.06	4.17	0.71	0.74	11.15	2.77	53.05	0.04	0.70
AH 168FE-RED	1992	1085	S	CELS-044	4	CELS-044	2.47	11.40	1.35	0	6.22	9.39	0.00	4.12	0.71	0.98	10.80	2.82	48.30	0.00	0.67
AH 168FE-OX	1996	1130	S	CELS-068	4	CELS-068	3.29	12.00	1.29	0	0.38	16.98	0.03	4.00	0.68	0.96	13.80	2.72	42.50	0.00	0.71
AH 200AL	1988	929	S	CELS-022	1	CELS-158	13.85	10.30	0.56	0.002	0.02	3.95	3.29	2.58	1.25	2.60	10.90	0.55	47.70	1.76	0.04
AH 200AL	1992	845	S	CELS-044	4	CELS-044	13.40	10.20	0.54	0	0.06	4.40	3.12	2.65	1.25	2.49	10.60	0.61	48.40	1.70	0.03
AH 200AV(AH-8)	1985	996	S	CELS-009	4	CELS-038	5.88	10.10	0.69	0.018	0.29	11.28	3.08	3.17	1.20	2.68	9.76	0.97	49.00	1.32	0.09
AH 200AV	1988	997	S	CELS-022	6	CELS-158	5.16	10.24	0.88	0.005	0.08	11.21	3.18	2.71	1.27	2.75	10.10	1.00	49.22	1.58	0.06
AH 200AV	1992	985	S	CELS-044	4	CELS-044	5.14	10.30	0.63	0	0.08	11.81	3.18	2.68	1.22	2.55	9.77	1.02	49.50	1.41	0.02
AH 200FE-RED	1988	1126	S	CELS-022	1	CELS-158	1.39	10.35	0.97	0.008	6.01	9.92	3.31	2.49	1.27	1.03	11.00	2.74	47.40	1.85	0.05
AH 200FE-RED	1992	1065	S	CELS-044	4	CELS-044	2.07	10.10	0.92	0	5.90	9.84	3.15	2.59	1.21	0.95	10.60	2.57	47.40	1.78	0.02
AH 200FE	1992	1070	S	CELS-076	4	CELS-044	2.07	10.10	0.92	0	5.90	9.84	3.15	2.59	1.21	0.95	10.60	2.57	47.40	1.78	0.02

Sample ID	Year Melted	T _L (°C)	Phases	T _L Reference	Chemical Analysis Replicates	Chemistry Reference ^{††}	Al ₂ O ₃	B ₂ O ₃	CaO	Cr ₂ O ₃	FeO	Fe ₂ O ₃	K ₂ O	Li ₂ O	MgO	MnO	Na ₂ O	NiO	SiO ₂	TiO ₂	Others
AH 200FE-RED-A	1992	1088	S	PNNL-avg	4	CELS-044	2.07	10.10	0.92	0	5.90	9.84	3.15	2.59	1.21	0.95	10.60	2.57	47.40	1.78	0.02
AH 202AL	1988	959	S	CELS-022	1	CELS-158	13.70	7.53	0.40	0.004	0.07	3.81	3.45	4.28	1.30	2.64	7.56	0.56	52.15	1.77	0.06
AH 202AL	1992	965	S	CELS-044	4	CELS-044	13.90	7.42	0.41	0	0.19	4.19	3.32	4.18	1.28	2.51	7.34	0.62	52.40	1.71	0.03
AH 202AV (AH-10)	1985	965	S	CELS-044	4	CELS-038	5.14	7.59	0.68	0.011	0.14	11.14	3.09	4.44	1.11	2.67	6.83	0.96	54.20	1.30	0.11
AH 202AV	1988	967	S	CELS-022	2	CELS-158	4.98	7.55	0.72	0.003	0.08	11.66	3.45	4.37	1.31	2.67	6.75	0.96	53.30	1.41	0.06
AH 202AV	1992	1010	S	CELS-044	4	CELS-044	4.96	7.44	0.72	0	0.14	11.75	3.33	4.27	1.30	2.59	6.55	1.00	54.10	1.37	0.03
AH 202FE-RED	1988	1123	S	CELS-022	2	CELS-158	1.38	7.32	1.01	0.008	6.88	9.86	3.47	4.20	1.31	1.04	7.73	2.87	51.00	1.84	0.08
AH 202FE-RED	1992	1110	S	CELS-044	4	CELS-044	1.36	7.08	0.96	0	6.90	8.93	3.28	4.27	1.26	0.95	7.62	2.73	52.50	1.72	0.02
AH 202FE	1992	1160	S	CELS-076	4	CELS-044	1.36	7.08	0.96	0	6.90	8.93	3.28	4.27	1.26	0.95	7.62	2.73	52.50	1.72	0.02
AH 202FE-RED-A	1992	1123	S	PNNL-avg	4	CELS-044	1.36	7.08	0.96	0	6.90	8.93	3.28	4.27	1.26	0.95	7.62	2.73	52.50	1.72	0.02
AH 202FE-OX	1996	1100	S	CELS-068	4	CELS-068	0.99	7.34	1.36	0	0.62	15.31	3.26	4.36	1.31	0.96	7.77	2.66	50.10	1.75	0.02
AH-5-1985#	1985	991	S	CELS-009	4	CELS-038	5.48	6.95	0.66	0.002	0.19	11.19	3.16	3.77	0.60	2.64	9.24	0.96	53.08	1.31	0.01
AH-9-1985#	1985	1000	S	SS	4	CELS-038	6.04	8.75	0.69	0.013	0.16	11.43	3.13	3.47	0.58	2.64	9.20	0.97	50.88	1.33	0.11
AH-13 -1985#	1985	1096	S	CELS-009	4	CELS-038	6.48	6.41	1.25	0.011	0.06	13.53	3.06	3.32	0.49	3.25	8.80	1.14	49.00	1.29	0.13
AH-16-1985#	1985	1073	S	CELS-009	4	CELS-038	6.36	7.20	1.26	0.077	0.19	13.19	3.06	4.06	1.00	3.22	6.54	1.10	50.20	1.30	0.11
DWPF SF (10/26/87)	1987	1066	S	CELS-024	6	CELS-025	4.59	8.49	1.45	0.091	0.19	13.89	2.68	3.22	0.86	1.93	11.50	1.10	48.10	1.16	0.26
DWPF SF (10/28/87)	1987	1062	S	CELS-024	6	CELS-025	4.67	8.66	1.44	0.096	0.19	14.00	2.69	3.32	0.81	1.89	11.60	1.11	47.60	1.21	0.15
DWPF SF (10/27/87)	1987	997	S, C(?)	CELS Letter (5-3-89)	6	CELS-025	4.53	8.37	1.51	0.090	0.19	14.08	2.74	3.21	0.86	1.97	11.50	1.11	48.00	1.16	0.23
DWPF SF (10/27/87)	1987	1012	S	CELS-024	6	CELS-025	4.53	8.37	1.51	0.090	0.19	14.08	2.74	3.21	0.86	1.97	11.50	1.11	48.00	1.16	0.23
Frit 165 (Nominal)	1984	732	T+X	CELS-001	---	CELS-001	0.00	8.49	0.00	0	0	0.00	0.00	6.86	0.96	0.00	12.80	0.00	70.08	0.00	0.80
IDMS 165 Black Frit	1988		S	CELS Letter (5-3-89)	6	CELS-025	4.62	6.84	1.58	0	0.16	11.43	0.13	4.94	0.75	1.96	11.20	0.84	54.40	0.23	0.83

DWPF STATISTICALLY DESIGNED COMPOSITION MATRIX

Sample ID	Year Melted	T _L (°C)	Phases	T _L Ref	Chem Reps	Chem Ref. ^{††}	Al ₂ O ₃	B ₂ O ₃	CaO	Cr ₂ O ₃	FeO	Fe ₂ O ₃	K ₂ O	Li ₂ O	MgO	MnO	Na ₂ O	NiO	SiO ₂	TiO ₂	U ₃ O ₈
SG01	1996	1124	S	PNNL ⁹¹	2	90,91	2.50	10.23	1.98	0.09	0.19	13.95	3.79	5.89	0.49	0.97	6.22	2.13	42.71	0.65	4.48
SG02	1996	775 755	R, C C	PNNL ⁹¹	2	90,91	2.56	5.11	1.93	0.02	0.08	5.89	3.77	5.89	2.35	3.03	11.00	0.06	57.79	0.15	0.00
SG03	1996	1164	S	PNNL ⁹¹	2	90,91	3.95	9.42	1.52	0.24	0.16	11.62	2.07	3.41	1.88	2.41	9.90	1.56	46.64	0.28	3.52
SG04 [‡]	1996	1261	S	PNNL ⁹¹	2	90,91	8.28	4.89	0.32	0.08	0.20	14.50	1.49	5.99	2.58	0.96	6.17	2.06	51.75	0.16	0.26
SG05	1996	1084	S	PNNL ⁹¹	2	90,91	5.60	7.73	1.15	0.20	0.14	10.49	2.67	4.44	1.56	1.96	8.48	1.10	52.27	0.40	2.51
SG05B	1996	1082	S	PNNL ⁹¹	2	90,91	5.56	7.84	1.14	0.19	0.14	10.21	2.51	4.02	1.43	1.97	8.57	1.08	51.07	0.42	2.39
SG06	1996	911 931	R,S R,S	PNNL ⁹¹	2	90,91	7.90	5.01	2.00	0.09	0.19	14.06	3.77	2.97	0.50	0.98	10.95	0.05	47.93	0.65	0.26
SG07	1996	950	S	PNNL ⁹¹	2	90,91	8.11	10.62	0.31	0.29	0.04	5.77	3.64	5.43	2.29	2.91	6.03	0.06	53.29	0.17	0.26
SG08	1996	1114	R, S	PNNL ⁹¹	2	90,91	4.12	6.50	1.57	0.14	0.17	12.34	3.21	3.44	2.06	2.43	7.54	0.56	54.26	0.28	1.54
SG09	1996	1173	S	PNNL ⁹¹	2	90,91	8.21	10.11	2.01	0.28	0.20	14.62	1.51	5.78	0.52	0.98	6.30	0.05	43.96	0.16	4.81

Sample ID	Year Melted	T _L (°C)	Phases	T _L Reference	Chemical Analysis Replicates	Chemistry Reference ††	Al ₂ O ₃	B ₂ O ₃	CaO	Cr ₂ O ₃	FeO	Fe ₂ O ₃	K ₂ O	Li ₂ O	MgO	MnO	Na ₂ O	NiO	SiO ₂	TiO ₂	Others
SG10	1996	1098	R, S	PNNL ⁹¹	2	90,91	4.03	6.65	0.75	0.25	0.11	8.12	3.22	5.25	2.03	2.45	7.47	1.61	54.17	0.28	3.62
SG11	1996	895	R, S	PNNL ⁹¹	2	90,91	3.86	9.48	0.76	0.14	0.11	8.00	2.10	5.11	1.94	1.48	9.72	0.57	53.48	0.29	1.54
SG12	1996	1030	R, S	PNNL ⁹¹	2	90,91	2.59	5.01	0.32	0.28	0.13	14.53	1.50	3.04	2.48	0.97	11.14	0.04	56.35	0.16	0.27
SG13	1996	1063	R, S	PNNL ⁹¹	2	90,91	2.56	9.75	0.32	0.28	0.29	8.13	1.48	5.87	0.50	2.88	5.99	2.14	56.71	0.16	0.27
SG14	1996	951	S	PNNL ⁹¹	2	90,91	2.66	11.00	0.31	0.09	0.14	14.93	3.73	2.74	2.60	2.93	11.28	0.05	43.34	0.17	5.14
SG15	1996	935	R, C	PNNL ⁹¹	2	90,91	2.53	10.13	1.94	0.09	0.08	5.80	1.51	5.97	2.48	0.94	6.10	2.06	55.91	0.64	0.72
SG16	1996	995	R, S	PNNL ⁹¹	2	90,91	6.93	6.33	1.57	0.14	0.11	8.28	2.06	5.18	2.01	2.38	9.87	0.56	50.08	0.52	3.67
SG17	1996	1075	S	PNNL ⁹¹	2	90,91	3.97	7.92	1.59	0.14	0.17	12.19	3.23	5.32	0.98	1.45	9.98	1.59	45.72	0.53	3.58
SG18	1996	859 ^{‡‡}	S	PNNL ⁹¹	2	90,91	2.52	10.43	0.33	0.28	0.08	14.27	1.50	5.90	0.47	2.84	10.85	0.04	46.78	0.64	0.27
SG18B	1996	869 ^{‡‡}	R, S	PNNL ⁹¹	2	90,91	2.67	10.28	0.32	0.28	0.08	14.61	1.46	5.89	0.49	2.87	10.89	0.04	47.77	0.64	0.27
SG19	1996	929	S	PNNL ⁹¹	2	90,91	6.59	10.31	0.31	0.28	0.08	5.72	3.72	5.91	0.49	0.95	10.90	2.15	44.38	0.18	4.65
SG20	1996	799	R, S, C	PNNL ⁹¹	2	90,91	8.34	4.97	1.95	0.10	0.08	6.03	1.52	5.90	2.56	0.99	11.05	0.06	51.51	0.64	4.98
SG21	1996	987	R, S	PNNL ⁹¹	2	90,91	3.97	8.93	1.59	0.24	0.11	7.77	2.04	5.17	0.97	2.31	7.23	1.60	53.43	0.52	1.58
SG22	1996	1145	S	PNNL ⁹¹	2	90,91	6.94	6.54	1.53	0.25	0.17	12.57	2.10	5.19	1.01	1.46	9.84	1.58	50.01	0.28	1.61
SG23	1996	1069	R, S	PNNL ⁹¹	2	90,91	4.27	6.52	1.58	0.25	0.11	7.87	3.14	3.39	1.88	1.48	9.93	1.58	53.45	0.54	1.49
SG24	1996	995	R, C	PNNL ⁹¹	2	90,91	2.64	5.16	0.31	0.11	0.16	11.68	1.50	5.83	0.52	1.00	6.08	0.06	58.50	0.66	4.73
SG25 [‡]	1996	1310 1309	S S	PNNL ⁹¹	2	90,91	7.91	11.54	0.35	0.09	0.19	14.21	3.66	2.72	2.37	0.99	6.59	2.06	47.05	0.17	0.26
SG26	1996	1071	S	PNNL ⁹¹	2	90,91	4.07	6.69	0.77	0.24	0.17	12.35	2.07	3.75	1.00	1.46	10.07	0.58	52.27	0.52	3.66
SG27	1996	1086	S	PNNL ⁹¹	2	90,91	6.95	9.43	1.53	0.25	0.15	10.91	3.25	5.11	1.98	1.48	7.44	0.58	47.15	0.29	3.62
SG28	1996	833	R, C	PNNL ⁹¹	2	90,91	2.58	10.54	1.95	0.09	0.20	14.51	1.52	5.95	0.49	0.95	11.23	0.05	49.48	0.16	0.26
SG29	1996	811	S	PNNL ⁹¹	2	90,91	8.14	5.15	0.32	0.10	0.08	5.76	1.54	6.16	0.48	2.91	11.20	0.05	51.42	0.65	4.65
SG30	1996	1030	S	PNNL ⁹¹	2	90,91	8.03	5.09	1.92	0.10	0.08	5.81	3.67	5.37	2.37	2.85	10.90	2.06	44.10	0.18	4.50
SG31	1996	1081	S	PNNL ⁹¹	2	90,91	8.36	11.10	2.00	0.09	0.08	15.09	3.70	5.34	2.65	2.93	6.23	0.06	43.11	0.65	0.26
SG32 [‡]	1996	1132	S	PNNL ⁹¹	2	90,91	8.21	10.58	0.32	0.10	0.31	14.54	1.51	5.97	0.49	0.97	10.94	2.08	42.96	0.63	0.27
SG33	1996	943	S	PNNL ⁹¹	2	90,91	8.36	10.43	1.95	0.28	0.13	6.04	3.77	5.91	0.52	2.86	10.62	2.11	47.55	0.61	0.26
SG34 [‡]	1996	1282	S	PNNL ⁹¹	2	90,91	8.33	9.61	1.96	0.27	0.20	14.41	1.50	2.99	2.52	2.85	6.35	0.05	42.05	0.64	4.76
SG35 [‡]	1996	1231	S	PNNL ⁹¹	2	90,91	8.12	5.31	0.32	0.28	0.19	13.66	3.67	6.06	2.38	2.89	10.95	2.13	41.80	0.65	0.26
SG36	1996	813	R, C	PNNL ⁹¹	2	90,91	2.53	10.41	1.99	0.27	0.08	5.59	3.74	2.97	0.48	0.97	10.96	0.05	51.42	0.17	4.43
SG37	1996	944 945	R, S R, S	PNNL ⁹¹	2	90,91	2.63	10.29	1.96	0.30	0.11	5.67	3.83	5.88	2.40	0.98	6.04	0.32	58.23	0.66	0.26
SG38	1996	897	S	PNNL ⁹¹	2	90,91	2.67	11.13	0.32	0.09	0.20	14.50	3.71	2.71	2.57	2.97	11.28	0.06	43.29	0.65	5.07
SG39	1996	1164	S	PNNL ⁹¹	2	90,91	2.61	5.44	1.96	0.28	0.22	14.13	1.48	3.01	0.50	2.87	11.16	2.12	52.23	0.64	0.26
SG40	1996	1173	S	PNNL ⁹¹	2	90,91	8.20	10.80	0.31	0.29	0.08	5.86	1.44	2.65	2.39	0.97	10.96	2.08	46.93	0.66	4.71
SG41 [‡]	1996	1304	S	PNNL ⁹¹	2	90,91	8.10	11.12	1.98	0.08	0.20	14.32	1.61	2.75	0.52	2.94	6.52	2.02	42.42	0.18	4.90
SG42	1996	990	S	PNNL ⁹¹	2	90,91	4.55	9.15	0.74	0.23	0.16	12.04	3.23	5.10	1.94	2.41	9.78	0.57	45.99	0.54	1.58
SG43	1996	924	S	PNNL ⁹¹	2	90,91	6.77	8.80	0.73	0.15	0.11	7.95	3.23	3.77	0.98	2.45	9.69	0.58	51.54	0.28	1.61
SG44 [‡]	1996	1244	R, S	PNNL ⁹¹	2	90,91	7.00	9.19	0.74	0.15	0.17	12.59	2.13	3.71	1.98	1.46	7.55	1.59	51.02	0.53	1.67
SG45	1996	936	R, S, C	PNNL ⁹¹	2	90,91	2.61	10.56	1.96	0.10	0.08	5.72	1.53	2.96	2.43	2.94	10.80	2.14	55.89	0.17	0.26
SG46 [‡]	1996	1247	S	PNNL ⁹¹	2	90,91	2.65	5.22	0.31	0.28	0.20	14.59	3.88	5.85	2.49	0.99	6.46	2.10	49.20	0.64	4.90
SG47	1996	1144	S	PNNL ⁹¹	2	90,91	2.67	5.03	1.97	0.28	0.20	14.73	1.52	5.83	2.48	1.00	11.08	2.06	45.57	0.18	5.00

Sample ID	Year Melted	T _L (°C)	Phases	T _L Reference	Chemical Analysis Replicates	Chemistry Reference ††	Al ₂ O ₃	B ₂ O ₃	CaO	Cr ₂ O ₃	FeO	Fe ₂ O ₃	K ₂ O	Li ₂ O	MgO	MnO	Na ₂ O	NiO	SiO ₂	TiO ₂	Others
SG48	1996	862 847	C C	PNNL ⁹¹	2	90,91	2.71	9.84	0.31	0.09	0.08	5.63	3.73	2.96	0.48	0.97	10.70	2.13	56.70	0.65	0.26
SG49	1996	877	C	PNNL ⁹¹	2	90,91	2.91	5.08	0.31	0.10	0.11	7.93	3.72	5.28	0.51	2.89	6.20	0.07	59.53	0.18	4.69
SG50 [‡]	1996	1285	S	PNNL ⁹¹	2	90,91	2.65	5.42	1.98	0.28	0.20	14.71	3.72	3.02	0.50	2.89	6.30	2.10	49.32	0.64	4.81
SG51	1996	1033	R, S	PNNL ⁹¹	2	90,91	7.98	5.22	1.95	0.28	0.20	14.64	3.72	2.99	0.50	0.96	10.90	0.05	48.89	0.16	0.26

† Glasses in the shaded rows were excluded from Model Data since they did not have spinel as a primary phase; the primary phases identified were spinel (S), clinopyroxene (C), RuO₂ needles (R), Tridymite (T), and an unknown (X)

‡ Water quenched instead of quenched in air.

‡‡ Glasses SG18 and SG18B (which was referred to as SG52 by PNNL [91]) were measured for liquidus temperature additional times after using different preparation methods and furnaces. The additional values were 883, 879, 891, 883, 887, and 882°C for glass SG18 and 883, 882, 883, and 891°C for glass SG18B (or SG52) [91].

Table VI. Composition Regions Covered by the SRNL and PNNL Glass Data Sets

Oxide Species (wt%)	SRNL Extreme Matrix Compositions	PNNL SG Designed Matrix Compositions	Pooled Data Used in Modeling Liquidus
Al ₂ O ₃	0.99-14.16	2.50-8.36	0.99-14.16
B ₂ O ₃	6.41-12.65	4.89-11.54	4.89-12.65
CaO	0.38-1.58	0.31-2.01	0.31-2.01
Cr ₂ O ₃	0.0-0.96	0.08-0.30	0.00-0.30
FeO	0.02-6.90	N/A	0.02-6.90
Fe ₂ O ₃	3.43-16.98	5.78-15.17	3.43-16.98
(ΣFe) ₂ O ₃	3.45-17.60	5.78-15.17	3.45-17.60
K ₂ O	0.00-3.47	1.44-3.89	0.00-3.89
Li ₂ O	2.49-5.11	2.65-6.16	2.49-6.16
MgO	0.47-1.43	0.49-2.65	0.47-2.65
MnO	0.74-3.25	0.96-2.97	0.74-3.25
Na ₂ O	6.54-14.90	5.99-11.28	5.99-14.90
NiO	0.53-3.05	0.04-2.15	0.04-3.05
SiO ₂	42.50-55.30	41.80-58.23	41.80-58.23
TiO ₂	0.00-1.85	0.16-0.66	0.00-1.85
U ₃ O ₈	N/A	0.26-5.14	0.00-5.14
ZrO ₂	0.005-0.97	N/A	0.00-0.97

N/A the data set did not include glasses with reduced iron, ZrO₂, or U₃O₈

* The sum of the components used in the liquidus temperature model, constitute between approximately 81.6 and 94.5% of the glasses by weight.

Table VII Proposed Cation Substitutions for Waste Glass Quasicrystalline Complexes*

Pyroxene-like Precursor			Nepheline-like Precursor		Metasilicate or Disilicate Precursor	
MT IV CN	M1 VI CN	M2 VI-VIII CN	T1 IV CN	N1 VIII-IX CN	T2 IV CN	N2 VI-VIII CN
Si ⁴⁺			Si ⁴⁺		Si ⁴⁺	
Al ³⁺	Al ³⁺		Al ³⁺			Al ³⁺
Fe ³⁺	Fe ³⁺		Fe ³⁺			Fe ³⁺
	Ti ⁴⁺		Ti ⁴⁺			Ti ⁴⁺
	Cr ³⁺					Cr ³⁺
	Zr ⁴⁺					Zr ⁴⁺
	Ni ²⁺	Ni ²⁺				Ni ²⁺
	Mg ²⁺	Mg ²⁺				Mg ²⁺
	Mn ²⁺	Mn ²⁺				Mn ²⁺
		Ca ²⁺				Ca ²⁺
		K ⁺		K ⁺		K ⁺
		Li ⁺		Li ⁺		Li ⁺
		Na ⁺		Na ⁺		

- * Zn²⁺ is not included because it is not found in significant concentrations in waste glasses. Fe²⁺ was removed as its impact on liquidus temperature (T_L) is normally indistinguishable since T_L measurements are performed in air.
f CN is coordination number of the lattice site

Table VIII. Quasicrystalline Distribution in Waste Glass Just Prior to Crystallization*

	PYROXENE-LIKE PRECURSORS			NEPHELINE- LIKE PRECURSORS		SUM
	M2	M1	MT	N1	T1	
Al ₂ O ₃	0	0.0607	0.9393	0	0	1.0000
B ₂ O ₃	0	0	0	0	0	0.0000
CaO	0.029	0	0	0	0	0.0290
Cr ₂ O ₃	0	0.9202	0	0	0	0.9202
Fe ₂ O ₃	0	0.1079	0.0193	0	0.6094	0.7366
K ₂ O	0.3041	0	0	0.1049	0	0.4090
Li ₂ O	0.1745	0	0	0.1068	0	0.2813
MgO	0.0167	0.0223	0	0	0	0.0390
MnO	0.994	0.00603	0	0	0	1.0000
Na ₂ O	0.1671	0	0	0.2518	0	0.4189
NiO	0	0.1079	0	0	0	0.1079
SiO ₂	0	0	0.0193	0	0.0133	0.0326
TiO ₂	0	0.0568	0	0	0.5667	0.6235
U ₃ O ₈	0	0	0	0	0	0.0000
ZrO ₂	0	0.0458	0	0	0	0.0458

* Where the meta or disilicate contribution is SUM - (M2+M1+MT+N1+T1)

Table IX. Composition of the SCM-2 Glass (Frit 131 and Average SRS Stage 1 Waste)

Oxide	Electrode A	Electrode B	Electrode C	Electrode D	Average
Al ₂ O ₃	2.15	2.02	2.11	3.72	2.5
B ₂ O ₃	11.01	10.95	11.20	11.85	11.25
CaO	1.18	1.18	1.20	0.68	1.06
Cr ₂ O ₃	0.16	0.04	0.07	0.03	0.077
Fe ₂ O ₃ *	21.87	21.30	22.73	17.87	20.95
Li ₂ O	2.73	2.84	2.84	2.82	2.81
MgO	1.23	1.11	1.16	1.34	1.21
MnO	5.01	4.71	4.88	3.85	4.61
Na ₂ O	10.23	10.02	10.46	9.75	10.11
NiO	2.16	1.25	1.51	1.18	1.53
SiO ₂	38.53	38.68	40.24	37.44	38.72
TiO ₂	0.33	0.32	0.33	1.35	0.59
ZrO ₂	0.06	0.06	0.06	0.36	0.36
SUM	96.65	94.48	98.79	92.24	95.78

* all Fe was measured to be Fe⁺³ by Fe⁺²/ΣFe measurement

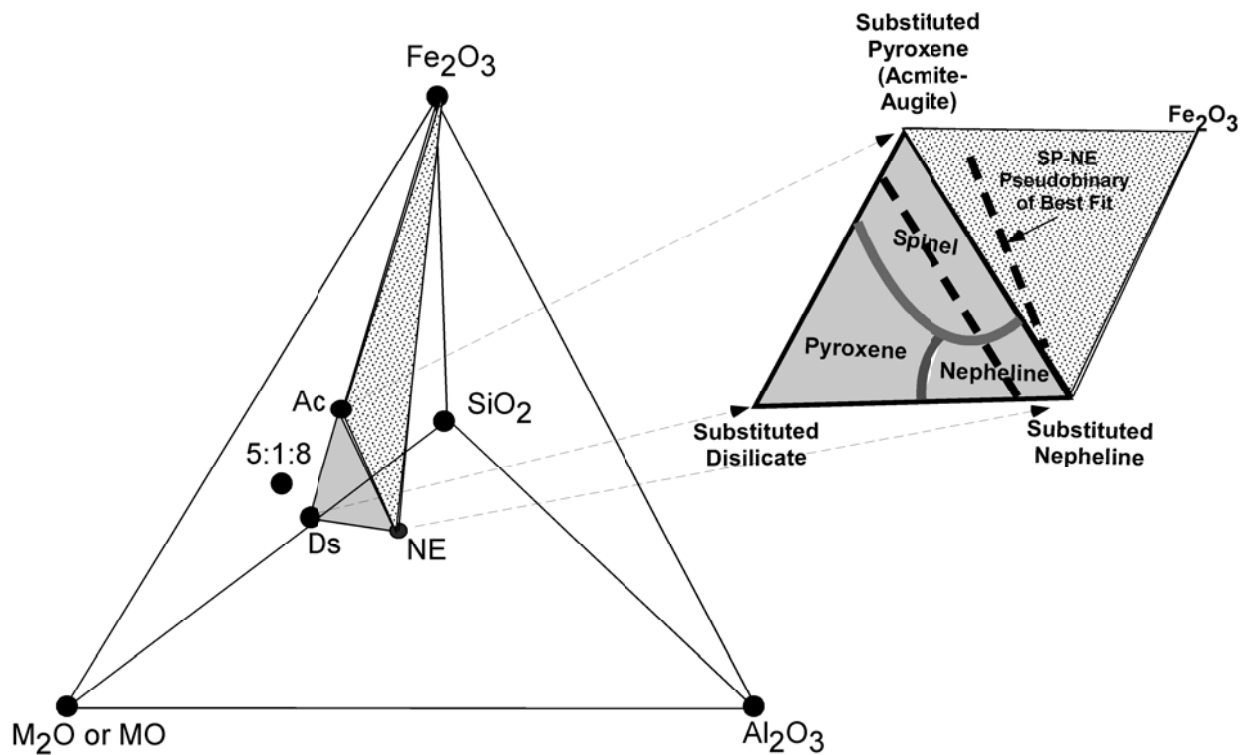


Figure 1. Quaternary System Fe_2O_3 - Al_2O_3 - SiO_2 -(M_2O or MO) after Reference 31 showing the position of the ternary system acmite(Ac)-nepheline(Ne)-Disilicate(Ds) that was used as a starting point for modeling the spinel-nepheline liquidus (indicated by the heavy dashed line in the ternary system inset). Note that Ac and Ne can also form pseudoternary systems with SiO_2 , with a 5:1:8 ($5Na_2O:Fe_2O_3:8SiO_2$) compound, and with Fe_2O_3 .

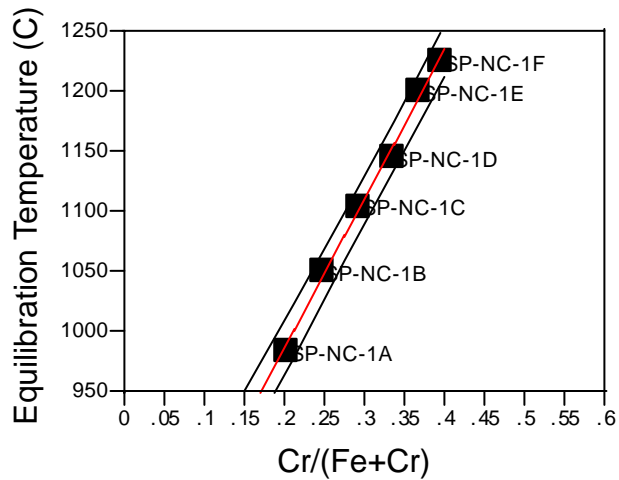


Figure 2. Variation of the composition of spinel in a simulated waste glass SP-NC-1 equilibrated at a variety of temperatures between 983°C and 1225°C. Note how the Cr solubility in the spinel increases with temperature. Data from Ref. 91.

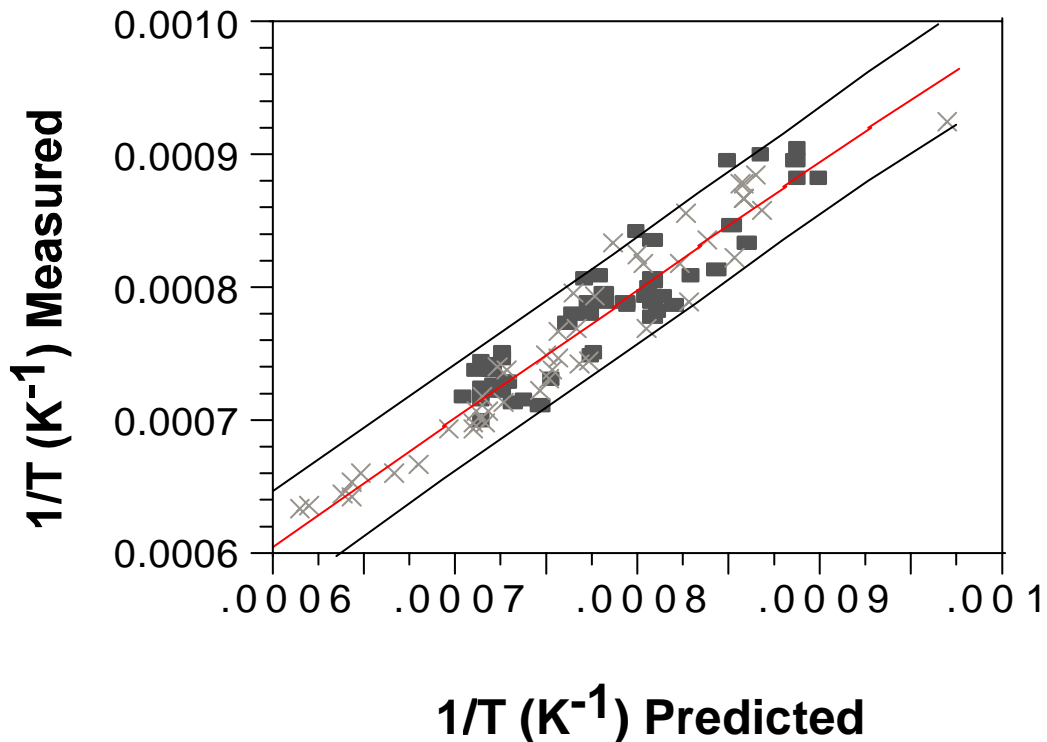


Figure 3. The relationship between reciprocal liquidus temperature (\bar{K}^1) and the quasicrystalline composition terms from Equation 21 for acmite (spinel) for the 105 statistically designed (X) and extreme (rectangle) model data. The dotted lines represent the 95% confidence curves about the fitted line.

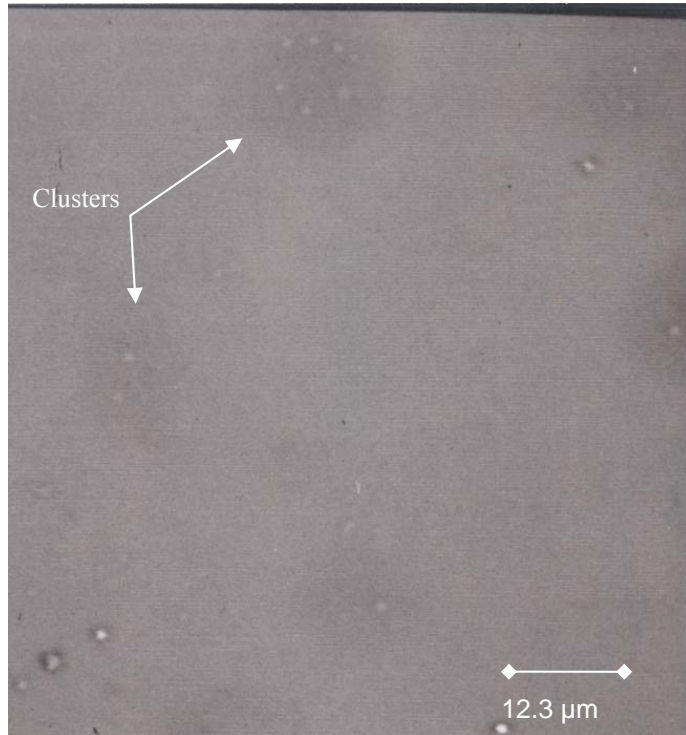


Figure 4. Scanning electron microscopy of 10-12mm clusters in an iron rich simulated waste glass. The Energy Dispersive Analysis by X-ray (EDAX) showed the clusters to be enriched in Al-Ti-K-Ca relative to the surrounding iron rich glass.

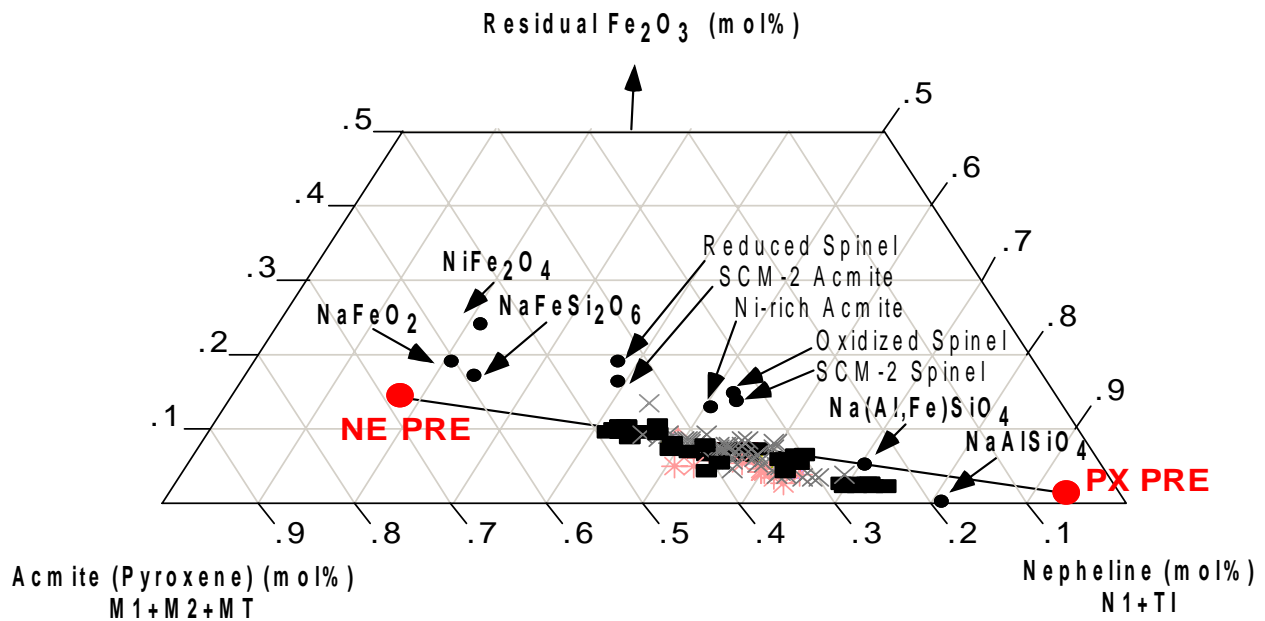


Figure 5. The pseudobinary diagram between the Ac precursor (MAlO_2 rich) and the Ne precursor (MFeO_2 rich) where M is any alkali (K, Na, Li). The positions of reference crystalline NiFe_2O_4 , acmite and nepheline species (large black circles) are plotted for reference as calculated in terms of the precursor compositions. Note the similarity of the positions of the NiFe_2O_4 spinel, and phase pure acmite ($\text{NaFeSi}_2\text{O}_6$) to the melt nepheline species and to pure NaFeO_2 and the similarity of crystalline nepheline to the melt pyroxene NaAlO_2 species. One hundred fifty nine data points are shown including the 105 model data, the Li et. al.[55] nepheline liquidus data and validation data from West Valley iron rich waste glasses containing Ce_2O_3 and ThO_2 [90]. Some of the analyzed spinel and acmite compositions from Table II are also added for reference as calculated in terms of the precursor end members and excess Fe_2O_3 .

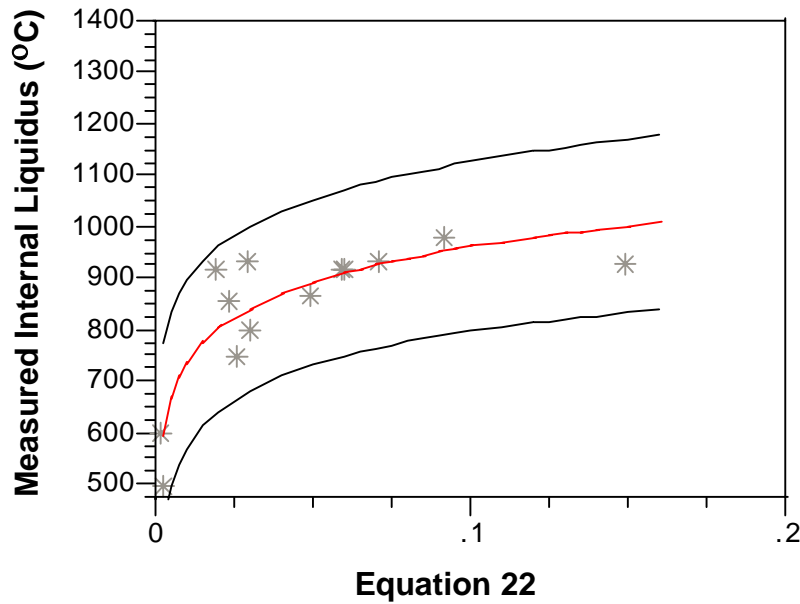
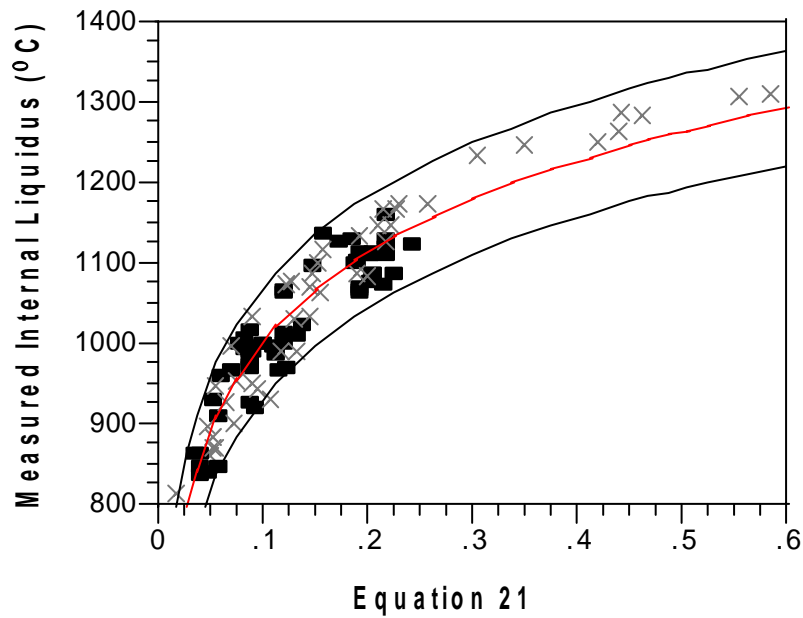


Figure 6. Fit of Equation 21 and Equation 22 to the measured model data for the internal spinel liquidus data modeled and the nepheline liquidus data of Li and others as given in the text. The solid rectangles are the SRNL Extreme Composition data for spinel crystallization, the X are the PNNL Designed Composition data for spine crystallization, the * are the Li, et. al. [55] plus TTT data for nepheline crystallization [22,37,100].

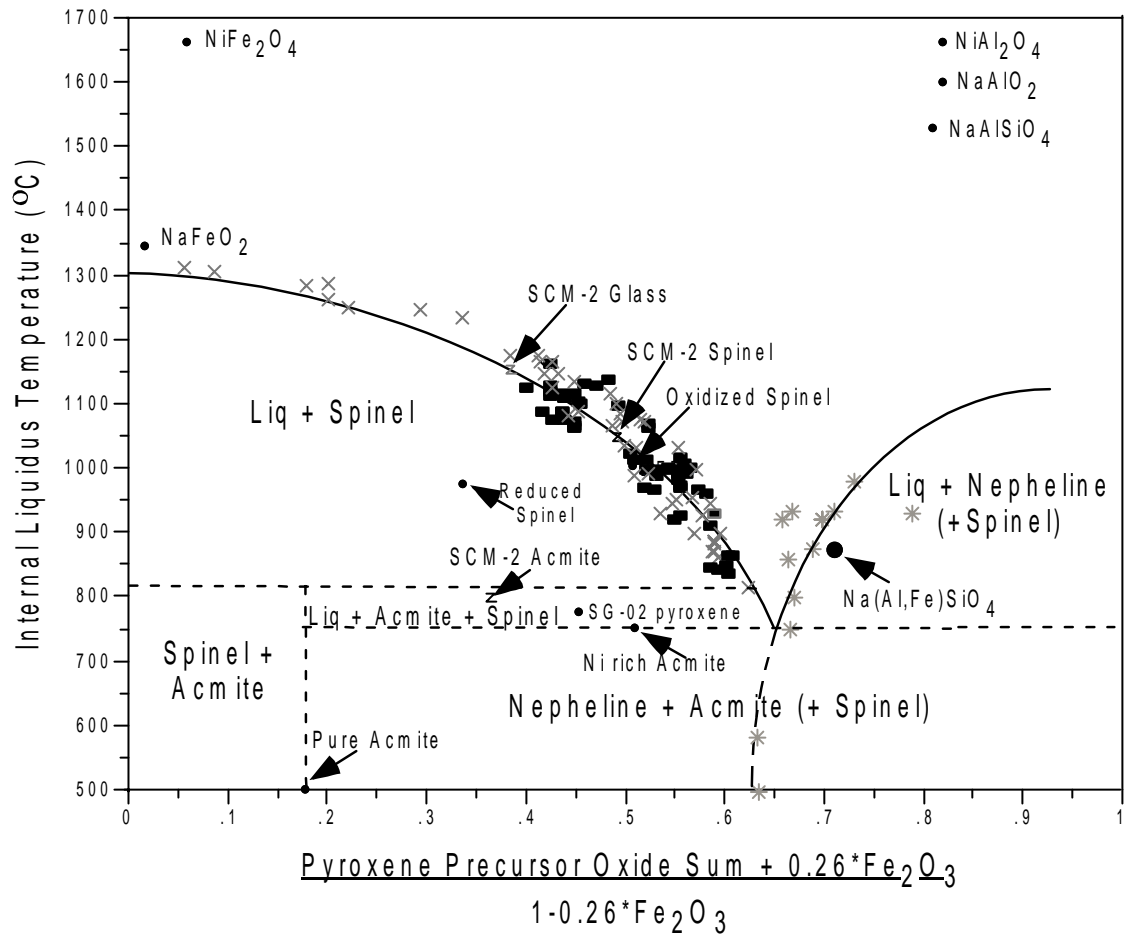


Figure 7. Pseudobinary phase diagram between acmite and nepheline expressed in terms of the pyroxene and nepheline precursor compositions (un-normalized mol%) given in Table VIII. Liquidus curves are fit to the measured liquidus data with Equation 21 and Equation 22 in order to generate the logarithmic fit (curvature) of the liquidus surfaces. Pure end member compositions are fit in terms of the pyroxene and nepheline precursor compositions adjusted for the position of the pseudobinary in the acmite-nepheline- Fe_2O_3 pseudoternary. All subsolidus phase assemblages coexist with lithium disilicates (LiSiO_3 and/or $\text{Li}_2\text{Si}_2\text{O}_5$) which is found to crystallize at long times and temperatures $<750^\circ\text{C}$ [21,22,37,38].

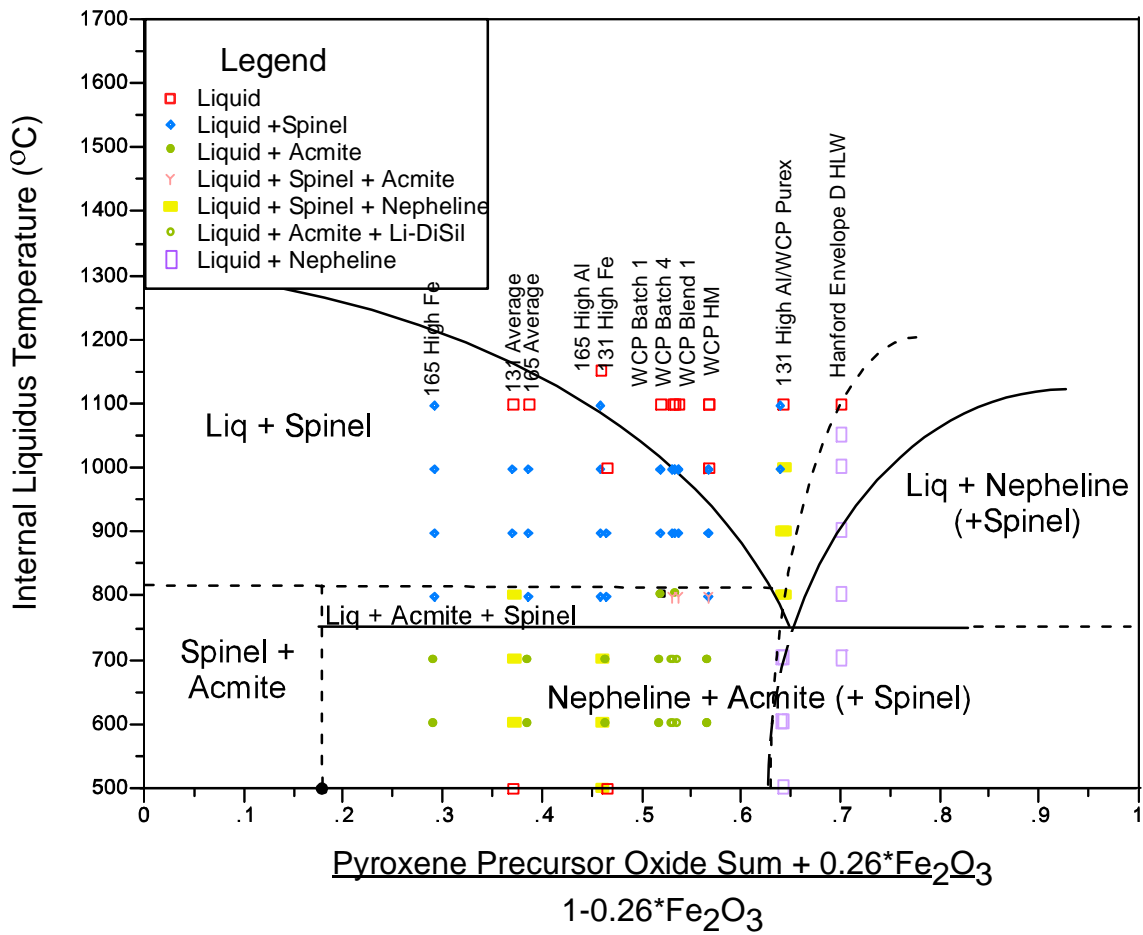


Figure 8. Pseudobinary phase diagram between acmite and nepheline expressed in terms of the pyroxene and nepheline precursor compositions. The data from time-temperature-transformation curves generated in References 21,22,37, and 38 are overlain for validation.

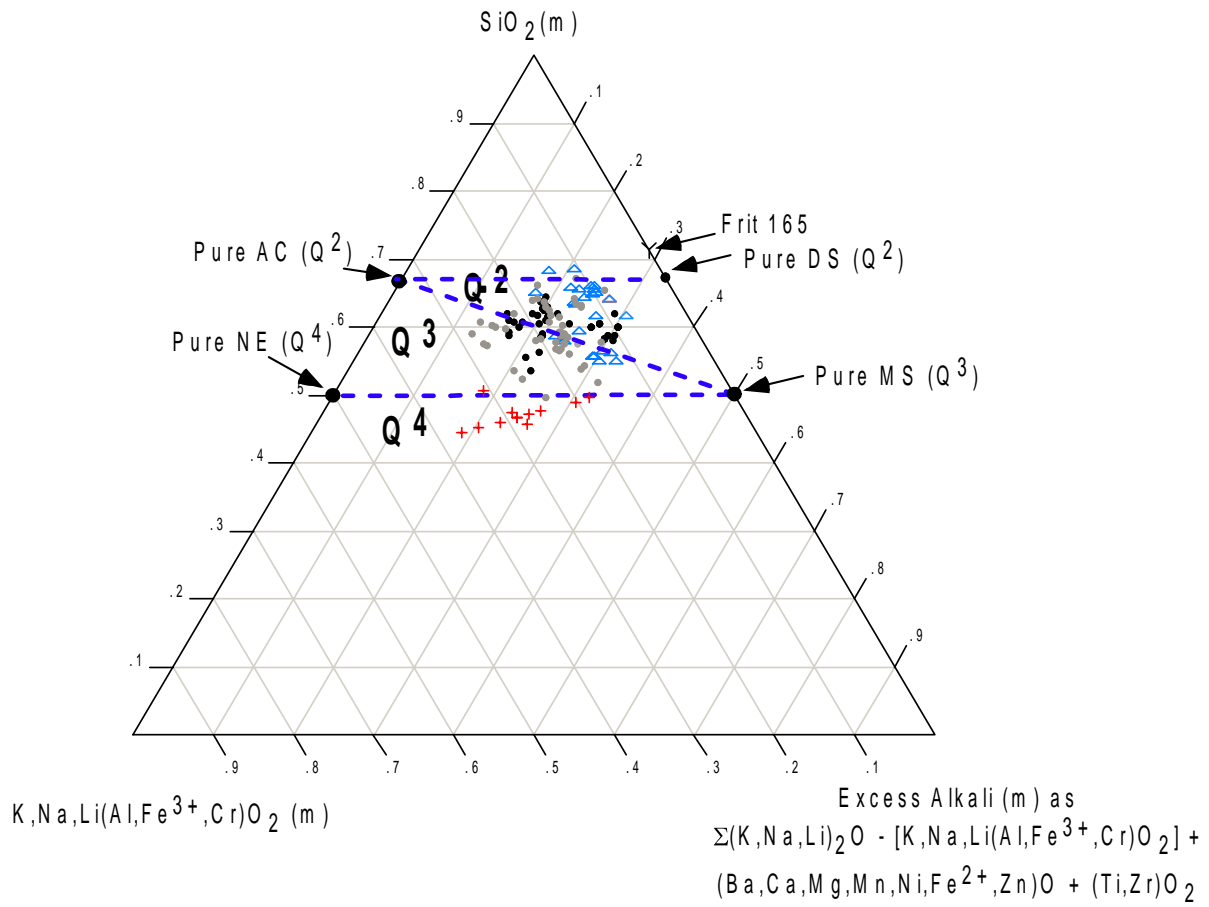


Figure 9. The relation of melt polymerization to the crystallization of nepheline (+), spinel (●), and pyroxenes (clino- and ortho-, ▲) as liquidus phases.

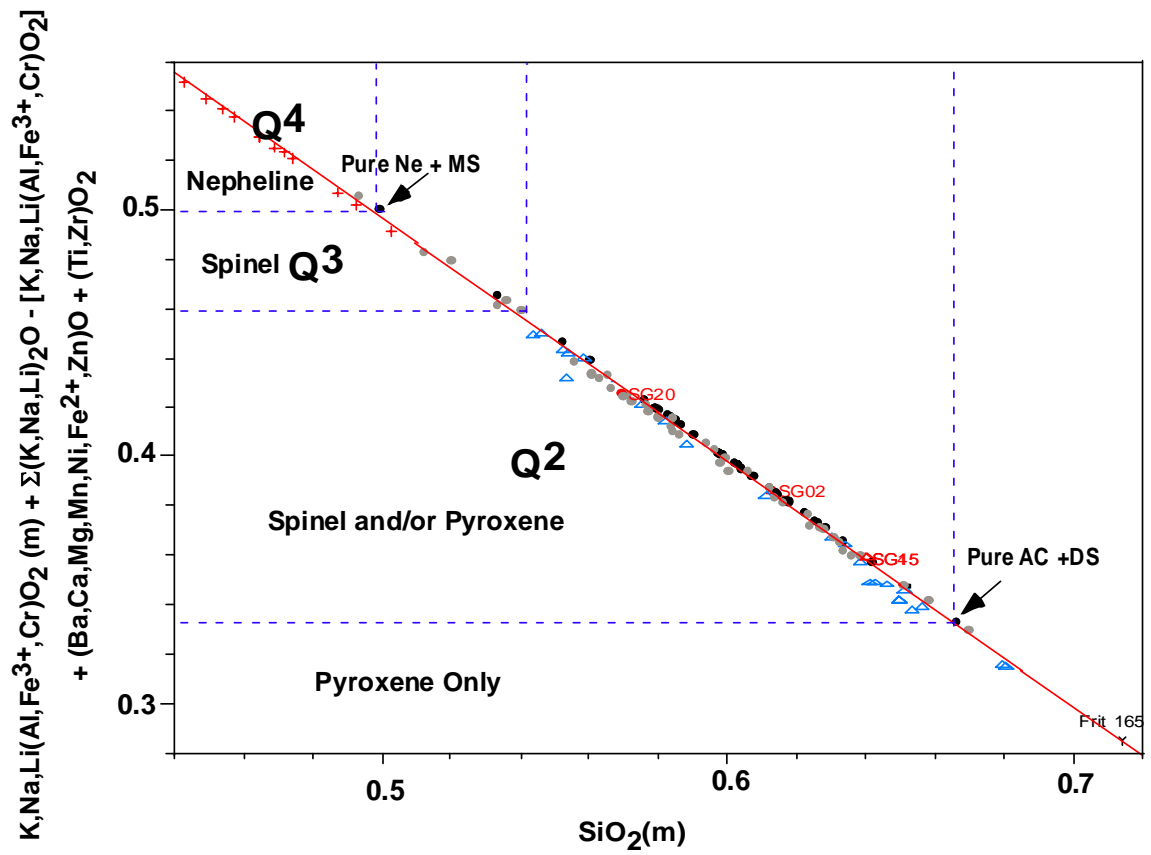


Figure 10. Two dimensional representation of the role of melt polymerization on crystallization of nepheline (+),spinel (•), and pyroxenes (clino- and ortho-, ▲) as liquidus phases.

REFERENCES

- 1 R.A. Palmer and S.M. Barnes, **“Vitrification Status Report for the West Valley Demonstration Project,”** *Ceram. Trans.* 107, 353-362 (2000).
- 2 T.J. Rowland, G.P. Rudy and J.D. Wagoner, **“Vitrification: A Success Story in 1997 Across the DOE Complex,”** in *Waste Management 98*, Paper #14-01, University of Arizona, Tucson, AZ (1998).
- 3 J.T. Carter, R.E. Edwards, J.E. Occhipinti, R.S. Beck and D.C. Iverson, **“Defense Waste Processing Facility (DWPF) Radioactive Operations – Year Two,”** in *Waste Management 98*, Paper #14-03, University of Arizona, Tucson, AZ (1998).
- 4 M. Colder and J. Palmer **“The Treatment of Wastes at Sellafield for Safe Storage and Disposal,”** in *Waste Management 98*, Paper #12-04, University of Arizona, Tucson, AZ (1998).
- 5 R. Liberge, J.L. Desvaux, D. Pageron and C. Saliceti, **“Industrial Experience of HLW Vitrification at La Hague and Marcoule,”** in *Waste Management 98*, Paper #14-05, University of Arizona, Tucson (1998).
- 6 H. Masson, J.L. Desvaux, E. Pluche and A. Jouran in *Global 99*, Proceedings of the International Conference on Future Nuclear Systems, American Nuclear Society, La Grange, IL (1999).
- 7 J. Fleisch, W. Grunewald, W. Lumpp, K.G. Roth and W. Tobie, **“Status of Planning and Licensing of the German HLLW Vitrification Plant,”** in *Waste Management 98*, Paper #14-07, University of Arizona, Tucson, AZ (1998).
- 8 R.L. Postles and K.G. Brown, **“The DWPF Product Composition Control System at Savannah River: Statistical Process Control Algorithm,”** *Nuclear Waste Management IV*, G.G. Wicks, D.F. Bickford, and L.R. Bunnell (Eds.), *Ceramic Transactions*, V. 23, American Ceramic Society, Westerville, OH, 559-568 (1991).
- 9 C.M. Jantzen and K.G. Brown, **“Statistical Process Control of Glass Manufactured for the Disposal of Nuclear and Other Wastes,”** *Am. Ceramic Society Bulletin*, 72, 55-59 (May, 1993).
- 10 C.M. Jantzen, **“Relationship of Glass Composition to Glass Viscosity, Resistivity, Liquidus Temperature, and Durability: First Principles Process-Product Models for Vitrification of Nuclear Waste,”** *Nuclear Waste Management IV*, G.G. Wicks, D.F. Bickford, and L.R. Bunnell (Eds.), *Ceramic Transactions*, V. 23, American Ceramic Society, Westerville, OH, 37-51 (1991).

-
- 11 C.M. Jantzen, K.G. Brown, T.B. Edwards, J.B. Pickett, "**Method of Determining Glass Durability, THERMO™ (Thermodynamic Hydration Energy Model),**" U.S. Patent #5,846,278 (December, 1998).
 - 12 C.M. Jantzen, "**Method for Controlling Glass Viscosity (VISCOMP™),**" U.S. Patent #5,102,439 (April, 1992).
 - 13 C.M. Jantzen and K.G. Brown, LIQCOMP™ (patent in preparation).
 - 14 M.J. Plodinec, "**Long-Term Waste Management Progress Report Small-Scale Electric Melter, II. Slag Formation,**" U.S. DOE Report DPST-78-453, E.I. duPont deNemours & Co., Savannah River Laboratory, Aiken, SC (August, 1978).
 - 15 M.J. Plodinec and J.R. Wiley, "**Viscosity and Electrical Conductivity of Glass Melts as a Function of Waste Composition,**" Proceedings International Symposium on Ceramics in Nuclear Waste Management," CONF-790420, U.S. DOE, Cincinnati, OH, 210-212 (1979).
 - 16 M.J. Plodinec, "**Long-Term Waste Management Progress Report Small-Scale Electric Melter, IIV. Effects of Feed Mixing and Segregation on Glass Melting,**" DPST-79-227, E.I. duPont deNemours & Co., Savannah River Laboratory, Aiken, SC (January, 1979).
 - 17 G.G. Wicks and W.N. Rankin, "**Microstructural Analysis of Slag Formation in Battelle's Calcine Fed Ceramic Melter (CFCM),**" DPST-79-372, E.I. duPont deNemours & Co., Savannah River Laboratory, Aiken, SC (April, 1979).
 - 18 J.P. Mosely and M.B. Cospser, "**An Analysis of Spinel Deposition in the 1941 Melter,**" DPST-81-587, E.I. duPont deNemours & Co., Savannah River Laboratory, Aiken, SC (July, 1981).
 - 19 C.M. Jantzen, "**Lack of Slag Formation in the Scale Glass Melter,**" DPST-87-373, E.I. duPont deNemours & Co., Savannah River Laboratory, Aiken, SC (April, 1987).
 - 20 A. Paul, **Chemistry of Glasses**, Chapman & Hall, London, 293pp., (1982).
 - 21 D.F. Bickford and C.M. Jantzen, "**Devitrification of SRL Defense Waste Glass**", Sci. Basis for Nuclear Waste Management, VII, G.L. McVay (ed). Elsevier Publ., New York 557-565 (1984).
 - 22 D.F. Bickford and C.M. Jantzen, "**Devitrification of Defense Nuclear Waste Glasses: Role of Melt Insolubles,**" J. Non-Crystalline Solids ,84 [1-3], 299-307 (1986).
 - 23 P. Izak, P. Hrma, and M.J. Schweiger, "**Kinetics of Conversion of High-Level Waste to Glass,**" in Nuclear Site Remediation, P.G. Eller and W.R. Heineman (Eds.), ACS Symposium Series, v. 778, American Chemical Society, Washington, DC, 314-328 (2001).
 - 24 C.M. Jantzen, K.G. Brown, K.J. Imrich, and J.B. Pickett, "**High Cr₂O₃ Refractory**

Corrosion in Oxidizing Melter Feeds: Relevance to Nuclear and Hazardous Waste Vitrification,” *Environmental Issues and Waste Management Technologies in the Ceramic and Nuclear Industries*, Vol. IV Ceramic Transactions, v. 93, J.C. Marra and G.T. Chandler (Eds.), American Ceramic Society, Westerville, OH, 203-212 (1999).

- 25 ASTM C1174. Annual Book of ASTM Standards, Vol. 12.01: *Standard Practice for Prediction of the Long-Term Behavior of Materials, Including Waste Forms, Used in Engineered Barrier Systems (EBS) for Geological Disposal of High-Level Radioactive Waste*.
- 26 D.S. Kim and P. Hrma, **“Models for Liquidus Temperature of Nuclear Waste Glasses,”** *Environmental and Waste Management Issues in the Ceramic Industry, II*, D.F. Bickford et. al (Eds.), *Ceramic Trans.*, V. 45, 327-337 (1994).
- 27 D.S. Kim, P. Hrma, D.E. Smith, and M.J. Schweiger, **“Crystallization in Simulated Glasses from Hanford High-Level Nuclear Waste Composition Range,”** *Environmental and Waste Management Issues in the Ceramic Industry*, G.B. Mellinger (Ed.), *Am. Ceram. Soc.*, Westerville, OH 179-189 (1990).
- 28 P.R. Hrma, G.F. Peipel, M.J. Schweiger, D.E. Smith, D.S. Kim, P.E. Redgate, J.D. Vienna, C.A. LoPresti, D.B. Simpson, D.K. Peeler, M.H. Langowski, **“Property/Composition Relationships for Hanford High-Level Waste Glasses Melting at 1150°C, Vols. 1 and 2,”** U.S. DOE Report PNL-10359, Battelle Memorial Institute, Pacific Northwest Laboratory, Richland, WA (December, 1994).
- 29 P. Hrma, J.D. Vienna, M. Mika, J.V. Crum, G.F. Peipel, **“Liquidus Temperature Data for DWPF Glass,”** U.S. DOE Report PNNL-11790, Pacific Northwest National Laboratory, Richland, WA (May, 1999).
- 30 M.J. Plodinec, **“Solubility Approach for Modeling Waste Glass Liquidus,”** *Sci. Basis for Nuclear Waste Mgt.*, XXII, D.J. Wronkiewicz and J.H. Lee (Eds.), *Materials Research Society*, Pittsburgh, PA 223-230 (1999).
- 31 D.K. Bailey and J.F. Schairer, **“The System Na₂O-Al₂O₃-Fe₂O₃-SiO₂ at 1 Atmosphere, and the Petrogenesis of Alkaline Rocks,”** *Journal of Petrology*, 7, Part 1, 114-170 (1966).
- 32 J. Nolan, **“Melting Relations in the System NaAlSi₃O₈-NaAlSiO₄-NaFeSi₂O₆-CaMgSi₂O₆-H₂O, and their Bearing on the Genesis of Alkaline Undersaturated Rocks,”** *Q. Jour. Geol. Soc. London*, 122, 119-157 (1966).
- 33 C.M. Jantzen and K.G. Brown, **“Impact of Phase Separation on Waste Glass Durability,”** *Environmental Issues and Waste Management Technologies in the Ceramic and Nuclear Industries*, V, G. T. Chandler (Eds.), *Ceramic Transactions*, V. 107, 289-300 (2000).
- 34 C.M. Jantzen and J.M. Pareizs, **“Glass Durability Modeling: The Role of Activated Complexes and Quasi-Crystalline Structural Ratios,”** WSRC-MS-2004-00663 (submitted)

to J. Nucl. Mat.).

- 35 J.D. Vienna, *ASTM Standard Test Methods for Determining the Liquidus Temperature (TL) of Waste Glasses and Simulated Waste Glasses, in preparation*
- 36 ASTM C829. Annual Book of ASTM Standards, Vol. 15.02: *Standard Practices for Measurement of Liquidus Temperature of Glass by the Gradient Furnace Method*
- 37 C.A. Cicero, S.L. Marra, and M.K. Andrews, **“Phase Stability Determinations of DWPF Waste Glasses,”** U.S. DOE Report WSRC-TR-93-227, Rev. 0, Westinghouse Savannah River Company, Aiken, SC 74pp., (May 1993).
- 38 Andrews, M.K., Cicero, C.A., Marra, S.L., Beam, D.C. and Jantzen, C.M., **“Phase Stability Determinations of DWPF Waste Glasses,”** Nucleation and Crystallization in Liquids and Glasses, Ceramic Transactions, v.30, 371-374 (1993).
- 39 L. Bragg and G.F. Claringbull, **“Crystal Structure of Minerals,”** The Crystalline State, Vol. IV, G. Bell and Sons, Ltd., London, 409pp. (1965).
- 40 W.A. Deer, R.A. Howie, and J. Zussman, **“Rock-Forming Minerals, V.5 Non-Silicates,”** John Wiley & Sons, New York, 363pp., (1962).
- 41 A. Navrotsky and O.J. Kleppa, **“The Thermodynamics of Cation Distributions in Simple Spinels,”** J. Inorgan. Nucl. Chem., 29, 2701-2714 (1967).
- 42 C.M. Jantzen, D.F. Bickford, and D.G. Karraker, **“Time-Temperature-Transformation Kinetics in SRL Waste Glass,”** Advances in Ceramics, 8, American Ceramic Society, Westerville, OH, 30-38 (1984).
- 43 M. Mika, M.J. Schweiger, J.D. Vienna, and P. Hrma, **“Liquidus Temperature of Spinel Precipitating High-Level Waste Glasses,”** Sci. Basis for Nuclear Waste Mgt., XX, W.J. Gray and I.R. Triay (Eds.), Materials Research Society, Pittsburgh, PA 71-78 (1997).
- 44 H. Li, B. Jones, P. Hrma, J.D. Vienna, **“Compositional Effects on Liquidus Temperature of Hanford Simulated High-Level Waste Glasses Precipitating Nepheline (NaAlSiO₄),”** Environmental Issues and Waste Management Technologies in the Ceramic and Nuclear Industries, III, D.K. Peeler and J.C. Marra (Eds.), Am. Ceram. Soc., Westerville, OH, 279-288 (1998).
- 45 H. Li, P.Hrma, J.D. Vienna, M. Qian, Y. Su, D.E. Smith, **“Effects of Al₂O₃, B₂O₃, Na₂O, and SiO₂ on Nepheline Formation in Borosilicate Glasses: Chemical and Physical Correlations,”** J. Non-Crystalline Solids, 331, 202-216 (2003).
- 46 W.A. Deer, R.A. Howie, and J. Zussman, **“Rock-Forming Minerals, V.4 Framework Silicates,”** John Wiley & Sons, New York, 435 pp., (1963).

-
- 47 G. Donnay, J.F. Schairer, and J.D.H. Donnay, "**Nepheline Solid Solutions,**" Mineral. Mag., 32 [245]93-109 (1959).
- 48 D.A. Duke, J.F. McDowell, and B.R. Karstetter, "**Crystallization and Chemical Strengthening of Nepheline Glass-Ceramics,**" J. Am. Ceram. Soc., 50, 67-75 (1967).
- 49 W.A. Deer, R.A. Howie, and J. Zussman, "**Rock-Forming Minerals, V.2 Chain Silicates,**" John Wiley & Sons, New York, 379pp., (1963).
- 50 M.F.J. Flower, "**Phase Relations of Titan-Acmite in the System Na₂O-Fe₂O₃-Al₂O₃-TiO₂-SiO₂ at 1000 Bars Total Water Pressure,**" Am. Mineralogist, 59, 536-548 (1974).
- 51 A.C. Buechele, X. Feng, H. Gu, and I.L. Pegg, "**Alteration of Microstructure of West Valley Glass by Heat Treatment,**" Sci. Basis for Nuclear Waste Mgt., XIII, V.M. Oversby and P.W. Brown (Eds.), Materials Research Society, Pittsburgh, PA, 393-402 (1990).
- 52 I. Joseph, T.V. Palmiter and L.D. Pye, "**Phase Stability of Simulated Nuclear Waste Glass,**" Proceedings of Third International Conference on High Level Waste Management, Vol. 1, American Nuclear Society, La Grange Park, IL, 911-916 (1992).
- 53 J.V. Crum, M.J. Schweiger, P. Hrma, and J.D. Vienna, "**Liquidus Temperature Model for Hanford High-Level Waste Glasses with High Concentrations of Zirconia,**" Sci. Basis for Nuclear Waste Mgt., XX, W.J. Gray and I.R. Triay (Eds.), Materials Research Society, Pittsburgh, PA 79-85 (1997).
- 54 J.D. Vienna, P. Hrma, J.V. Crum, and M. Mika, "**Liquidus Temperature-Composition Model for Multi-Component Glasses in the Fe, Cr, Ni, and Mn Spinel Primary Phase Field,**" (Draft Revision 5).
- 55 H. Li, J.D. Vienna, P. Hrma, D.E. Smith and M.J. Schweiger, "**Nepheline Precipitation in High-Level Waste Glasses: Compositional Effects and Impact on the Waste Form Acceptability,**" Sci. Basis for Nuclear Waste Mgt., XX, W.J. Gray and I.R. Triay (Eds.), Materials Research Society, Pittsburgh, PA 261-268 (1997).
- 56 T.M. Besmann, K.E. Spear, and E.C. Beahm, "**The Assessment of Nepheline Precipitation in Nuclear Waste Glass Via Thermochemical Modeling,**" Sci. Basis for Nuclear Waste Management, V.XXIII, R.W. Smith and D.W. Shoesmith (Eds.), Materials Research Society, Pittsburgh, PA 715-720 (2000).
- 57 A.D. Pelton, "**Thermodynamic Modeling and Phase Equilibrium Calculations in Nuclear Materials,**" Pure & Appl. Chem., 69, 2245-2252 (1997).
- 58 A.D. Pelton and M. Blander, "**Thermodynamic Analysis of Ordered Liquid Solutions by a Modified Quasichemical Approach-Application to Silicate Slags,**" Met. Trans. B, 17B, 805-813 (1986).

-
- 59 M. Blander and A.D. Pelton, "**Thermodynamic Analysis of Binary Liquid Silicates and Prediction of Ternary Solution Properties by Modified Quasichemical Equations,**" *Geochim. Cosmochim. Acta*, 51, 85-95 (1987).
- 60 J.M. Welch, R.L. Miller, and J.E. Flinn, "**Immobilization of Three-Mile Island Core Debris,**" *Nuclear Waste Management*, G.G. Wicks and W.A. Ross (Eds.), *Advances in Ceramics*, V. 8, American Ceramic Society, Columbus, OH, 611-618 (1984).
- 61 G.E. Brown, Jr., F. Farges, and G. Calas, "**X-Ray Scattering and X-Ray Spectroscopy Studies of Silicate Melts,**" *Structure, Dynamics and Properties of Silicate Melts*, J.F. Stebbins, P.F. McMillan, and D.B. Dingwell (Eds.), *Reviews in Mineralogy*, V.32, 317-410 (1995).
- 62 C.W. Burnham, "**The Nature of Multicomponent Aluminosilicate Melts,**" *Phys. Chem. of the Earth*, v13 & 14, 191-227 (1981).
- 63 R.J.P. Williams, "**Deposition of Trace elements in Basic Magmas,**" *Nature*, v.184, 144 (1959).
- 64 P.L. Roeder, "**Activity of Iron and Olivine Solubility in Basaltic Liquids,**" *Earth and Planetary Sci. Letters*, 23, 397-410 (1974).
- 65 E. Takahashi, "**Partitioning of Ni²⁺, Co²⁺, Fe²⁺, Mn²⁺, and Mg²⁺ between olivine and silicate melts: Compositional Dependence of Partition Coefficients,**" *Geochim. Cosmochim. Acta* 42, 1829-1844 (1978).
- 66 E.A. Porai-Koshits, **The Structure of Glass**, p.25, Consultants Bureau, NY (1958).
- 67 W.H. Zachariasen, "**The Atomic Arrangement in Glass,**" *J. Am. Chem. Soc.*, v.54, 3841-3851 (1932).
- 68 W.H. Zachariasen, "**The Vitreous State,**" *J. Chem. Phys.* v. 3, 162-163 (1933).
- 69 B.E. Warren, "**X-ray Diffraction of Vitreous Silica,**" *Zeit. Krist.* v. 86, 349-358 (1933).
- 70 A.C. Wright, "**Neutron Scattering from Vitreous Silica, V. The structure of Vitreous Silica: What have we Learned from 60 years of Diffraction Studies?,**" *J. Non-Crystalline Solids*, v. 179, 84-115 (1994).
- 71 G.N. Greaves, "**EXAFS and the Structure of Glass,**" *J. Non-Crystalline Solids*, 71, 203-217 (1985).
- 72 M.Taylor and G.E. Brown, "**Structure of mineral glasses-II. The SiO₂-NaAlSiO₄ Join,**" *Geochim. et. Cosmochim. Acta*, v, 43, p.1467-1479 (1979).

-
- 73 F. Farges and G.E. Brown, **“Coordination Chemistry of Trace Levels of Zr, Mo, Th and U in Synthetic Silicate Melts and Natural Glasses-An In-situ, High-Temperature XAFS Spectroscopy Study,”** EOS Transactions, Am. Geophysical Union (1995a).
- 74 B.O. Mysen, **“Structure and Properties of Silicate Melts,”** Developments in Geochemistry, 4, Elsevier, New York 354pp (1988).
- 75 E.D. Lacy, **“A Statistical Model of Polymerisation/depolymerisation relationships in Silicate Melts and Glasses,”** Phys. Chem. Glasses, 6[5], 171-180 (1965).
- 76 R.M. Smart and F.P. Glasser, **“Silicate Anion Constitution of Lead Silicate Glasses and Crystals,”** Phys. Chem. Glasses, 19[5], 95-102 (1978).
- 77 K.D. Keefer, **“Phase Separation and Crystallization Phenomena in Silicate Systems,”** Unpublished PhD Thesis, Stanford University, 159p.(November, 1980).
- 78 P.C. Hess, **“Thermodynamic Mixing Properties and the Structure of Silicate Melts,”** in Thermodynamic Modeling of Geological Materials: Minerals, Fluids, and Melts Reviews in Mineralogy, v.32, Mineralogic Society of America, Washington, DC, 145-189 (1995).
- 79 A.J.G. Ellison and A. Navrotsky, **“Thermochemistry and Structure of Model Waste Glass Compositions,”** Sci. Basis for Nuclear Waste Management, XIII, V.M. Oversby and P.W. Brown (Eds.) Materials Research Society, Pittsburgh, PA, 193-207 (1990).
- 80 P. Izak, P. Hrma, J.S. Young, J. Klouzek, **“Evolution of Crystalline Phases During High Level Waste Feed-to-Glass Conversion,”** Ceramic Transactions, 119, Amer. Ceramic Soc., Westerville, OH, 509-515 (2001).
- 81 J.W. Hastie, E.R. Plante, and D.W. Bonnell, **“Vaporization of Simulated Nuclear Waste Glass,”** NBSIR 83-2731, National Bureau of Standards, Washington, DC (June, 1983).
- 82 D.W. Bonnell, E.R. Plante, and J.W. Hastie, **“Vaporization of Simulated Nuclear Waste Glass,”** J. Non-Crystalline Solids, 84, 268-275 (1986).
- 83 R.G.C. Beerkens, **“Modeling the Kinetics of Volatilization from Glass Melts,”** J. Am. Ceram. Soc. 84[9], 1952-1960 (2001).
- 84 H. Li, Y. Su, J.D. Vienna, and P. Hrma, **“Raman Spectroscopic Study - Effects of B₂O₃, Na₂O, and SiO₂ on Nepheline (NaAlSiO₄) Crystallization in Simulated High Level Waste Glasses,”** Environmental Issues and Waste Management Technologies, V, G.T. Chandler and X. Feng (Eds.), Ceramic Trans. 107, 469-477 (2000).
- 85 D. J. Stein and F.J. Spera, **“Molecular Dynamics Simulations of Liquids and Glasses in the System NaAlSiO₄-SiO₂: Methodology and Melt Structures,”** Am. Min. 80, 417-431 (1995).

-
- 86 C. Nelson, T. Furukawa, and W.B. White, **“Transition Metal Ions in Glasses: Network Modifiers or Quasi-Molecular Complexes?”** *Mat. Res. Bull.*, 18, 959-966 (1983).
- 87 E. W. Baumann. **“Colorimetric Determination of Iron (II) and Iron (III) in Glass,”** *Analyst*, v.117, 913-916 (1992).
- 88 R.F. Crow, J.D. Connolly, **“Atomic Absorption Analysis of Portland Cement and Raw Mix Using Lithium Metaborate Fusion,”** *Jour. Test. Evaluation*, 1, 382, 1973; ASTM C1463. Annual Book of ASTM Standards, Vol. 12.01: *Practice for Dissolving Glass Containing Radiactive and Mixed Waste for Chemical and Radiochemical Analysis*; ASTM C1317. Annual Book of ASTM Standards, Vol. 12.01: *Standard Practice for Dissolution of Silicate or Acid-Resistant Matrix Samples*.
- 89 Ramsey, W.G. and Schumacher, R.F. **“Effects of Formate and Nitrate on Waste Glass Redox at High Copper Concentration,”** U.S. DOE Report WSRC-TR-92-242, Westinghouse Savannah River Company, Aiken, SC (October 1992).
- 90 K.G. Brown, C.M. Jantzen, and G. Ritzhaupt, **“Relating Liquidus Temperature to Composition for Defense Waste Processing Facility (DWPF) Process Control,”** U.S. DOE Report WSRC-TR-2001-00520, Rev. 0, Westinghouse Savannah River Company, Aiken, SC (October 2001).
- 91 P. Hrma, J.D. Vienna, M. Mika, J.V. Crum, G.F. Piepel, **“Liquidus Temperature Data for DWPF Glass,”** U.S. DOE Report PNNL-11790, Pacific Northwest National Laboratory, Richland, WA (May, 1999).
- 92 H.D. Schreiber and A.L. Hockman, **“Redox Chemistry in Candidate Glasses for Nuclear Waste Immobilization,”** *J. Am. Ceram. Soc.*, 70[8], 591-594 (1987).
- 93 A. Navrotsky, **“Models of Crystalline Solution,”** in *Thermodynamic Modeling of Geological Materials: Minerals, Fluids, and Melts*, Reviews in Mineralogy, V. 17, Min. Soc. Amer., Washington, D.C., 35-69 (1987).
- 94 N.L. Bowen and J.F. Schairer, **“The Fusion Relations of Acmite,”** *Am. J. Sci*, 18, 365-374 (1929).
- 95 N.L. Bowen, J.F. Schairer, and H.W. V. Willems, **“The Ternary System: Na₂SiO₃-Fe₂O₃-SiO₂,”** *Am. J. Sci.*, 20, 405-455 (1930).
- 96 K. Yagi, **“Liquidus Data on the System Acmite-Nepheline-Diopside at 1 Atmosphere,”** *Carnegie Institute of Washington Year Book (C.I.W.Y.B.)* 62, Annual Report of the Director of the geophysical Laboratory, Carnegie Institution of Washington, Washington, DC, 133-134 (1963).
- 97 K. Kugimiya, E. Hirota, and Yoshichica Bando, **“Magnetic Heads Made of A Crystal-Oriented Spinel Ferrite,”** *IEEE Trans. On Magnetics*, 10 [3],907-909 (1974).

-
- 98 Rockware, Inc ® website: www.rockware.com.
- 99 I. N. Levine. **Physical Chemistry**, 2nd Ed., McGraw-Hill Book Company, New York, 1983.
- 100 W.G. Ramsey, “**Glass Dissolution Chemistry of the System Na₂O-B₂O₃-SiO₂-Al₂O₃-Fe₂O₃-CaO**,” Unpublished Ph.D. Thesis Clemson University, 202pp (1995).
- 101 Duratek Rept on Envelope D glass TTT Personal Communication
- 102 W.D. Kingery, H.K. Bowen, and D.R. Uhlmann, Introduction to Ceramics, 2nd edition, John Wiley & Sons, New York (1976).
- 103 W. Vogel, “**Chemistry of Glasses**,” Translation by N. Kreidl, The American Ceramic Society, Westerville, OH, 324pp (1985).
- 104 P. Gordon, “**Principles of Phase Diagrams in Materials Systems**,” McGraw-Hill Book Company, New York, 232pp. (1968).
- 105 I. Yasui, H. Hasegawa, and M. Imaoka, “**X-ray Diffraction Study of the structure of Silicate Glasses, Part I. Alkali Metasilicate Glasses**,” Phys. Chem. Glasses 24, 65-71 (1983).
- 106 M. Imaoka, H. Hasegawa, I. Yasui, “**X-ray Diffraction study of the Structure of Silicate Glasses, Part 2. Alkali Disilicate Glasses**,” Phys. Chem. Glasses 24, 72-78 (1983).
- 107 I. Yasui, Y. Akasaka, H. Inoue, “**Re-examination of Detailed Structure of Alkali Silicate Glasses Based on Two Types of Diffraction Data**,” J. Non-Crystalline Solids, 177, 91-96 (1994).
- 108 J. Schneider, V.R. Mastelaro, E.D. Zanotto, B.A. Shakhmatkin, N.M. Vedishcheva, A.C. Wright, H. Panepucci, “**Qⁿ Distribution in Stoichiometric Silicate Glasses: Thermodynamic Calculations and ²⁹Si High Resolution NMR Measurements**,” J. Non-Crystalline Solids, 325, 164-178 (2003).
- 109 L.A. Chick, G.L. McVay, G.B. Mellinger, and F.P. Roberts, “**Annual Report on the Development and Characterization of Solidified Forms for Nuclear Wastes, 1979**,” U.S. DOE Report PNL-3465, Battelle Memorial Institute, Pacific Northwest Laboratory, Richland, WA (December, 1980).
- 110 R.P. Turcotte, J.W. Wals, and R.P. May, “**Devitrification of Nuclear Waste Glasses**,” Sci. Basis for Nuclear Waste Mgt., II, C.J.M. Northrup, Jr. (Ed.), Plenum Press, New York, 141-146 (1980).

-
- 111 D. McPherson, I. Joseph, A. Mathur, C. Capozzi, S. Armstrong, and L.D. Pye, **“The Influence of Waste Variability on the Properties and Phase Stability of the West Valley Reference Glass,”** U.S. DOE Report DOE/NE/44139-29 (October, 1986).
- 112 I. Joseph, A. Mathur, C. Capozzi, J. Shegal, D. Butts, D. McPherson, L.D. Pye and L. Eisenstatt, **“Crystallization Behavior of a Fully Simulated West Valley Borosilicate Glass,”** Waste Management 88, Vol. 2, 487-491 (1988).
- 113 M.J. Schweiger, J.D. Vienna, and P. Hrma, **“Liquidus Temperature of Spinel Precipitating High-Level Waste Glasses,”** Sci. Basis for Nuclear Waste Mgt., XX, W.J. Gray and I.R. Triay (Eds.), Materials Research Society, Pittsburgh, PA 71-78 (1997).
- 114 H. Li, personal communication